Journal of Polymers and the Environment (2022) 30:833–854
https://doi.org/10.1007/s10924-021-02239-7

ORIGINAL PAPER

Development of Nanocomposite Films Based on Chitosan and Gelatin Loaded with Chitosan-Tripolyphosphate Nanoparticles: Antioxidant Potentials and Applications in Wound Healing

Sawssen Hajji[1] · Naourez Ktari[1,2] · Riadh Ben Salah[3] · Sami Boufi[4] · Frédéric Debeaufort[5,6] · Moncef Nasri[1]

Accepted: 5 July 2021 / Published online: 19 July 2021

Abstract
Recently, there is an increasing interest to prepare wound healing agents based on bio-polymers, due to their non-toxicity, biocompatibility and biodegradability. Despite this interest, nanocomposite films were prepared based on chitosan and gelatin reinforced with chitosan-sodium tripolyphosphate nanoparticles (CS-NPs). Nanoparticles were incorporated onto films at different weight ratios (2, 4 and 6 wt%, dry base). Nanocomposite films enriched with nanoparticles were characterized by a higher UV-barrier property, compared to the control film. Films were characterized in terms of physical, mechanical and thermal properties, as well as their bioactivity. An increase in the tensile strength was observed with CS-NPs incorporation, while the elongation at break was adversely affected by nanoparticles amount. Thermal analyses confirmed the compatibility and miscibility between the different film components. Further, CS-NPs addition increased the surface wettability (polar component and surface free energy) of nanocomposite films. The biological properties of films, as well as their wound healing ability were explored. Results showed that nanoparticles incorporation improved significantly the antioxidant and antibacterial efficacies of nanocomposite films. Moreover, *in-vivo* wound healing test showed that the rate of wound reduction was greatly elevated with a rapid re-epithelialization for treated group with nanocomposite films. Consequently, films were suitable and promising alternatives biomaterials for wound healing and skin regeneration.

Keywords Chitosan · Nanoparticles · Nanocomposite films · Structural and thermal properties · Antioxidant and antibacterial activities · Wound healing

Introduction

The survival and health of the human body depend mainly upon the strength and effectiveness of the immune system, the most important constituent of which is the skin. Acting as the first defense line confronting the external environment, skin represents the main barrier against the invasions of exogenous substances and/or organisms, thus any damage to the skin results in unexpected flaw in the immune system [1]. Various injuries that lead to second and third-grade burns with high levels of problems can endanger the lives of a large number of people. In these cases, often infections and microbial accumulations in burn wounds lead to a lot of problems and, even in some cases, it leads to death of the patient. Therefore, the production of a suitable coating to repair skin lesions with high antimicrobial ability and also to absorb pus and infection is very important. Indeed, the wound repair is an extremely complex mechanism that requires the coordination between many series of cellular

✉ Sawssen Hajji
hajjisawssen@yahoo.fr

1 Laboratory of Enzyme Engineering and Microbiology, National School of Engineering of Sfax (ENIS), University of Sfax, PB 1173, 3038 Sfax, Tunisia

2 Department of Life Sciences, Faculty of Science of Gabes, 6029 Gabès, Tunisia

3 Laboratory of Microorganisms and Biomolecules, Centre of Biotechnology of Sfax, 3018 Sfax, Tunisia

4 Faculty of Science of Sfax - LMSE, University of Sfax, 3018 Sfax, Tunisia

5 Univ. Bourgogne Franche-Comté - Agrosup Dijon, UMR PAM A02-102, 1 Esplanade Erasme, 21000 Dijon, France

6 Dpt of Bioengineering, IUT Dijon-Auxerre, Université de Bourgogne, PB 17867, 21078 Dijon Cedex, France

responses. Therefore, many scientific reports focused on the mechanisms of wound healing to develop biomaterials and dressings that could be applied in order to keep a clean wound, to protect wound against bacterial infections, and to enhance the wound healing process [2, 3].

Recently, there is a major interest to develop biopolymer matrices that can be used as wound dressings to enhance and accelerate the healing process. Indeed, the wound dressings act as a physical barrier, increase the permeability to oxygen invasion and moisture, and could protect the wounds against infection via microorganisms and viruses [4, 5]. In the last decades, many synthetic, hybrid and natural materials were used to prepare the wound dressings. In order to accelerate and accomplish the healing process, rapid progress has been made in the field of biomaterial applications in different industries and various types of natural and synthetic polymers have been used in different medical fields and especially as wound dressings. The bio-dressings were mostly designed due to their interesting gas permeability, controlled water vapor evaporation and wound exudates absorption, as well as their non-toxicity and especially their biodegradability. Among kinds of wound dressings, bio-based dressings were prepared based on biocompatible and biodegradable polymers, both natural and synthetic ones. Indeed, natural polymers, such as chitosan [6], cellulose [7], alginate and animal proteins, such as gelatin and collagen [8] were used for the wound healing treatments and in wound dressing preparation, due to their biocompatibility, non-cytotoxicity and hydrophilicity. Baek et al. [9] developed wound healing dressings using gelatin and catechin, characterized by an excellent biocompatibility and high antioxidant activity. They showed that those dressings blocked harmful external factors and was a good candidate for efficient wound treatment. Other study showed the effectiveness of alginate films enriched with Aloevera gel and cellulose nanocrystals as wound dressings, based on the in vitro cell viability, in vitro scratch wound and antibacterial studies [10].

Chitosan, a biopolymer of marine origin, has recently attracted attention due to its significant antimicrobial properties and the advantages of being non-toxic, biodegradable and biocompatible, as well as excellent film forming properties and strong antioxidant, anti-tumor and antiviral activities [11, 12]. Chitosan was extracted from shrimps, lobsters, krill, and crab shells waste. Due to its non-toxicity, biocompatibility and biodegradability, as well as the antioxidant and antimicrobial efficiencies, chitosan was used in various biomedical and pharmaceutical domains, especially in tissue engineering and wound healing.

Gelatin, a non-toxic, biodegradable and non-immunogenic bio-polymer was used in various biotechnological applications, especially in foods additives, biopackaging and in various biomedical and pharmaceutical domains. Being a derivative of collagen, gelatin exhibited a biocompatibility and thus attracts more attention as promising biomedical materials [13, 14]. Consequently, chitosan and gelatin combination gained much attention in numerous fields, including cosmetics, biomedical and pharmaceutical domains, as well as in foods industries. Such biomaterials could be used as coatings, biofilms, micro-capsules, biodegradable constructing materials and as wound dressings [15, 16].

Chitosan (CS), as well as the CS-based nanoparticles were widely used for biomedical materials including scaffolds, medical system development, drug diagnosis and orthopedic biomaterials, showing good biocompatibility through in vitro and in vivo tests. Many reports reported that chitosan-based dressings were suitable as wound dressings for dermal burns [17]. Thus, investigations of new wound dressings based on chitosan-nanoparticles promote and accelerate the wound healing process. Various chitosan-based nanomaterials were prepared using different method like ionic gelation, emulsion/reticulation, precipitation/coacervation, and polyelectrolyte complexation [18–20]. Among these techniques, ionic gelation method has been thoroughly used in order to obtain reproducible and nanometer size particles with narrow size distributions, as well as a highly positive surface charge. Chitosan nanoparticles could be used in different biotechnological and biomedical domains thanks to their functional and biological properties, higher specificity as proteins vectors, wound healing agents, anti-cancer agents, genes or antigens delivery [21]. Some studies focused on the effectiveness of wound dressings based on chitosan nanoparticles. Indeed, Shao et al. [22] showed that the silver nanoparticles incorporation enhanced the antibacterial efficacy of biomaterials and wound healing ability of the chitosan-based dressings. Zhao et al. [23] developed sericin blended chitosan nanofibers by electrospinning, which have huge potential for wound healing applications. Similarly, Yousefi et al. [24] developed chitosan nanofibers mats based on *Lawsonia inermis* (Henna) plant extract characterized by a high antibacterial and wound healing efficiencies.

Among the biological dressings, chitosan based nanocomposite films could be successfully used as antimicrobial dressings for improving the wound healing process, mainly due to their antimicrobial and antiviral efficiency, as well as their non-toxicity, biodegradability and biocompatibility properties. The aim of the present work was to prepare nanocomposite films based on crab chitosan and fish gelatin and enriched with CS-NPs. In order to improve the mechanical and biological properties of nanocomposite films, the as-prepared CS-NPs were blended with CS-gelatin mixture in different amounts. Films were tested for their antioxidant and antimicrobial activities, as well as wound healing efficiency.

Material and Methods

Reagents and Materials

Chitosan was obtained by chemical deacetylation of chitin extracted from crab (*Carcinus mediterraneus*) shells, as described in our previous study [25]. The deacetylation degree and molecular weight (MW) of chitosan were 80% and 1620 g/mol, respectively. Fish gelatin was extracted from golden grey mullet (*Liza aurata*) skin, as described by Bkhairia et al. [26] using crude acidic proteases from viscera of the same specie (*L. aurata*). Fish gelatin was characterized by a gel strength of 122.15 g and a MW at about 50,000 g/mol. Acetic acid, tripolyphosphate of sodium (TPP), diphenyl-1-picrylhydrazyl (DPPH) and 2,2'-azinobis(3-ethylbenzothiazoline-6-sulfonic acid) (ABTS) were purchased from Sigma Aldrich Chemical Co. USA.

Animals and Ethics

Adult wistar rats (male, weight between 150 and 200 g) used in this study were obtained from local Central Pharmacy in Sfax, Tunisia. Wistar rats were kept in an environmentally controlled breeding room at a room temperature of 22 ± 3 °C, a relative humidity level (RH) at about 55 ± 5% and a 12 h light–dark cycle. The experimental protocol was in accordance with the guidelines set Guide for the Care and Use of Laboratory of Animals issued by the University of Sfax in Tunisia and also approved by the Committee of Animal Ethics. The rats were then kept in individual cages in order to prevent the licking or the biting of wound areas by other wistar rats.

Chitosan Nanoparticles Preparation

CS-NPs were prepared by ionic gelation method. Firstly, chitosan was dissolved in acetic acid solution (2%, v/v) at 0.5% (w/v) and pH was adjusted to 4.5. Nanoparticles were spontaneously formed by adding 10 ml of TPP solution (0.7 mg/ml) slowly drop wise into the CS solution under a gentle stirring at room temperature (25 ± 1 °C) for 30 min. After this process, the prepared mixture was ultra-sonicated using an ultrasonic probe with diameter of 20 mm and 300 W high-intensity ultrasonic processor operating at 20 kHz for 5 min in ice bath to reduce the possible nanoparticles agglomeration. The resulted colloidal suspensions were then centrifuged at 10,000×*g* for 15 min at 4 °C, after that, the pellet was re-suspended in ultrapure water. The precipitate was washed twice to remove un-reacted substance, freeze-dried and then stored at 4 °C for further uses.

Nanoparticles and Gelatin Characterization

The nanoparticles size of the prepared CS-NPs was determined by Dynamic Light Scattering (DLS) method using Zeta-sizer-Nano-ZS (Malvern-Instrument, UK) at room temperature (25 ± 2 °C) and a scattering angle of 90°. Pure water was used as a reference for dispersing medium. Gelatin was characterized by Nuclear Magnetic Resonance (NMR) solid-state ^{13}C and ^{1}H-CP/MS spectroscopy by using a Brüker W300 spectrometer with a frequency of 75.5 MHz, 50 ms of acquisition time, 8 ms of contact time and a repetition time of 5 s.

Nanocomposite Films Preparation

The CS-NPs were used for the nanocomposite films preparation based on chitosan and fish gelatin at different amounts. Chitosan solution (2%, w/v) was prepared by dissolving chitosan powder into acetic acid solution 2% (v/v). Chitosan solution was mixed with fish gelatin (2%, w/v) solution with 1:1 ratio. Glycerol was added onto films as a plasticizer at 5% of dry weight. In parallel, CS-NPs were dispersed in diluted acetic acid solution (1%, w/v) by magnetic stirrer for 2 h, followed by sonication for 15 min using an ice bath. Different concentrations of CS-NPs dispersion (2, 4 and 6 wt%, dry base) were added to chitosan–gelatin mixture and stirred for 30 min at room temperature for the preparation of CS-TPP NF2, CS-TPP NF4 and CS-TPP NF6 films, respectively. Control film (CS-TPP NF0) was prepared with similar procedure without CS-NPs incorporation.

All films were obtained by casting a volume of 25 ml of film-forming solution in Petri dishes (13.5 cm diameter), drying in a ventilated climatic chamber (KBF 240 Binder, ODIL, France) at 25 °C and 50% of relative humidity (RH) for 48 h. Then films were peeled off and conditioned at 50% RH before the heating treatment and before all the analyses. For Fourier Transform Infrared (FTIR) and X-ray Diffraction (DRX) spectroscopies, as well as Differential Scanning Calorimetric (DSC), Dynamic Mechanical Analysis (DMA) and Thermogravimetric Analysis (TGA) analyses, films were conditioned at 0% RH prior experiments.

Characterization of Nanocomposite Films

Thickness, Swelling Degree and Water Solubility

Thickness of nanocomposite films was measured using a hand-held micrometer (Alton M820-25, China) with a sensitivity of 10 µm at six random positions for each film sample. The swelling degree was performed in order to determine water uptake ability of CS-TPP NFs. The dried films were weighed and then immersed in 20 ml of distilled water for 12 h at 25 ± 1 °C. After that, the excessive water on the

surface of films was removed with filter paper and then weighed immediately. The experiment measurement was repeated at least five times until the weight was constant. The swelling degree was calculated as follow:

$$\text{Swelling degree } (\%) = \frac{W_s - W_d}{W_d} \times 100$$

where W_d and W_s were the dried and wet films weights, respectively.

Water solubility was defined as the percentage of water-soluble dry matter of films that was dissolved after their immersion in the distilled water and was determined according to Hafsa et al. [27] method. For that, the nanocomposite films (2 cm × 2 cm), dried previously to a constant weight in a hot air oven at 105 °C, were weighed to determine the initial dry weight (W_1). The water solubility of films was measured from immersion of each film sample in distilled water (20 ml) for 24 h at 25 °C under a constant agitation. The residual film pieces were removed from water and dried at 105 °C to constant weight (W_2). The water solubility of nanocomposite films was calculated using the following equation:

$$\text{Water solubility } (\%) = \frac{W_1 - W_2}{W_1} \times 100$$

Ultraviolet–Visible (UV–Vis) Spectroscopy and Color Parameters Determination

The barrier properties of nanocomposite films against ultraviolet (UV) and visible lights were investigated using an UV–Visible spectrophotometer (SAFAS-UVmc) in the wavelength range of 200–800 nm. Films were cut into rectangle (1 cm × 3 cm) and directly placed in the spectrophotometer-test cell. Air was used as a reference.

Color of films was determined using a CIE colorimeter (CR-400; Konica Minolta, Japan). A white standard color plate ($L_0 = 97.5$, $a_0 = -0.1$, and $b_0 = 2.3$) was used as background for the color measurements of the films. Color of the films was expressed as L^* (lightness/brightness), a^* (redness/greenness) and b^* (yellowness/blueness) values. The difference in color (ΔE) of CS-TPP NFs as a function of CS-NPs content was calculated referred to the CS-TPP NF0 film, as follow:

$$\Delta E = \sqrt{(\Delta L)^2 + (\Delta a)^2 + (\Delta b)^2}$$

Mechanical Properties and Surface Morphology

The mechanical properties of films were determined using a Microelectronics Universal Testing Instrument Model TA (HD plus model, Stable Micro-Systems, UK). In order to determine tensile strength (TS, MPa), elastic modulus (EM, MPa) and elongation at break (EAB, %), films were cut into dumbbell-shaped pieces (2.5 cm × 8 cm) using a standardized precision cutter (Thwing-Albert JDC Precision Sample Cutter). All film samples were conditioned at 25 °C and a RH of 50% for 2 weeks before testing. The initial grip separation and cross-head speed were 50 mm and 50 mm/min, respectively. Measurements were carried out at room temperature (25 ± 1 °C) using six samples for each film formulation.

The surface morphology of nanocomposite films was determined using Scanning Electron Microscope SEM (Hitachi S800) at an angle of 90° to the surface, using different magnifications and operating at 25 kV.

Structural and Thermal Properties

The structural characterization of the prepared nanocomposite films was analyzed using two spectroscopy methods: Attenuated Total Infrared Reflectance (AT-IR) and X-Ray Diffraction (XRD). The IR measurements were performed using Perkin Elmer spectrometer (Spectrum-65, France) equipped with an Attenuated Total Reflectance accessory with a Zn-Se crystal. 32 scans were collected with 4 cm^{-1} resolution in the wavelength range of 4000–400 cm^{-1}. Calibration was done using background spectrum recorded from the clean and empty cell at room temperature. The XRD analysis of CS-TPP NFs was conducted with X-Ray diffractometer (D8-Advance Brüker XRD diffractometer, Germany) operated at 50 kV, 100 mA and 1.54 Å with Ni-filtered Cu-Kα radiation. The films were scanned from 2 θ angles of 5–80° range and at a scan speed of 0.5°/min. The crystallinity indices of nanocomposite films were determined according to method cited in our previous study [28].

Thermo-gravimetric Analysis (TGA) has been widely used to determine the thermal stability and thermal decomposition of films with increasing temperature. The thermal stability of CS-TPP NFs was studied using thermogravimetric analyzer (TGA-Q500 High-Resolution, TA. Instruments), and operating under a nitrogen flow to prevent the possible thermal oxidation. Temperature range was 25–600 °C at a heating rate of 5 °C/min. The weight of nanocomposite films, initially about 5 mg, was constantly measured with an accuracy of 0.01 mg. Data analysis was performed using TA Universal Analysis 2000 software (version 4.5 A, TA instruments).

Thermal properties of nanocomposite films were also studied using Differential Scanning Calorimeter (DSC Q20, TA-Instruments) equipped with a liquid nitrogen cooling system. The DSC method was also used to estimate the melting temperature and crystallization points, as well as the glass transition of nanocomposite films. Film samples

were accurately weighed into sealed aluminum pans. An empty capsule serves as an inert reference and the apparatus was calibrated using indium. The thermal profile of the nanocomposite films was analyzed in a temperature range of -50–150 °C at a heating rate of 10 °C/min and under a nitrogen flow rate of 25 ml/min. The glass transition temperature (*Tg*) for each sample was then determined from the mid-point of the second heating cycle using TA-Universal Analysis 2000 software (version 4.5 A, TA-instruments).

Dynamic mechanical analysis (DMA) was carried out using a Dynamic Mechanical Analyzer DMA PYRIS™ Diamond DMA (PerkinElmer, Waltham, MA, USA) with standard bending head at a frequency of 1 Hz in the range 25–170 °C and heating rate of 5 °C/min. In the DMA instrument, a film was longitudinally deformed by small sinusoidal stress. The resulting strain, which lags behind the applied force by phase angle δ, was measured. The values of the storage modulus *E* (inphase component), the loss modulus *E″* (out-of-phase component), and the loss tangent (*Tan* $\delta = E/E''$) were measured as function of temperature.

Surface Properties and Wettability

The surface properties and wettability of nanocomposite films were carried out using the sessile drop method on goniometer (Drop Shape Analyzer from KrussGmbH) equipped with image analysis software (ADVANCE) and determined by the contact angle, surface free energy (γ_{film}) and polar ($\gamma_{film}{}^{P}$) and dispersive ($\gamma_{film}{}^{D}$) components.

The surface free energy (γ_S), polar (γ_S^P) and dispersive (γ_S^D) components of nanocomposite films were estimated according to the Owens and Wendt [29] method using a series of standard solvents, with a known surface free energy and respective dispersive and polar components: water ($\gamma_L = 72.8$ mN/m; $\gamma_L^D = 21.8$ mN/m; $\gamma_L^P = 51$ mN/m), ethylene glycol ($\gamma_L = 47.7$ mN/m; $\gamma_L^D = 30.9$ mN/m; $\gamma_L^P = 16.8$ mN/m) and diiodomethane ($\gamma_L = 50.8$ mN/m; $\gamma_L^D = 50.8$ mN/m; $\gamma_L^P = 0$ mN/m). The surface free energy of films, as well as their dispersive and polar components was determined using the following equations:

$$\gamma_S = \gamma_S^P + S^D$$

$$\gamma_L(1+\cos\theta) = 2\left[\left(\gamma_S^D \times \gamma_L^D\right)^{1/2} + \left(\gamma_S^P \times \gamma_L^P\right)^{1/2}\right]$$

where the subscripts S and L refers to the solid (the film surface) and to the liquid (solvent), respectively.

The surface free energy, polar and dispersive components of nanocomposite films were determined from the linear regression of the Owens and Wendt plot with the three different solvents previously listed for 120 s.

Contact angle measurements were determined according to Karbowiak et al. [30] method using three different liquids (water, ethylene glycol and diiodomethane), with well-known polar γ_L^P and dispersive γ_L^D contributions. A droplet of each liquid (2 µl) was deposited on the film surfaces using a precision syringe. Then the contact angle was measured at t = 0 (< 2 s) and during 120 s. The both sides of drop were considered for contact angle value and averaged. Five replicates per film sample were carried out for each formulation. All tests were conducted in an environmental chamber at 25 ± 2 °C and 50% of RH. Water contact angle and drop volume were determined using three solvents (water, ethylene glycol and diiodomethane), with well-known polar γ_L^P and dispersive γ_L^D contributions as a function of time (0–120 s).

Biological Properties

Biological properties of nanocomposite films were studied by determining their antioxidant and antibacterial efficiencies. For the antioxidant activity, different tests, such as DPPH free radical-scavenging power, ferric-reducing power and β-carotene bleaching method, as described in a previous study [12] were tested. For the ABTS-radical scavenging activity, 10 mg of each film sample (cut into small pieces) was immersed in 1 ml of diluted ABTS solution. The mixture was left at room temperature in the dark for 1 h. After that, the absorbance was measured at 734 nm against the corresponding control using a spectrophotometer. The control was prepared in the same manner, except that distilled water was used instead of the film sample. The ABTS scavenging activity of film samples was determined as follows:

$$\text{ABTS} - \text{scavenging activity}\ (\%) = \frac{A_{control} - A_{sample}}{A_{control}} \times 100$$

where $A_{control}$ and A_{sample} were the absorbance control and the film samples, respectively.

The antibacterial activity of nanocomposite films was investigated against several infectious bacterial strains using a disc agar diffusion method. The microorganisms used were three Gram-positive bacteria (*Bacillus cereus*-ATCC 11778, *Staphylococcus aureus*-ATCC 25923 and *Micrococcus luteus*-ATCC 4698) and five Gram-negative bacteria (*Escherichia coli*-ATCC 25922, *Klebsiella pneumonia*-ATCC 13883, *Salmonella enteric*-ATCC 43972, *Salmonella typhimurium*-ATCC 19430 and *Enterobacter sp.*) strains. Culture suspension (100 µl) of the tested microorganisms (about 10^6 colony forming units (CFU)) was spread over the Luria Bertani (LB) agar. Films (1 cm × 1 cm) were firstly sterilized by UV-light during 30 min and then placed on the plate surfaces and incubated at 37 °C for 24 h. The appearance of a clear area below or around the films was seemed to be positive for antibacterial activity.

Wound Healing Efficiency

The in vivo wound healing efficiency of CS-TPP NF4 (enriched with 4 wt% of CS-NPs) as compared to CS-TPP NF0 (without nanoparticles incorporation) on the regeneration of the injured skin was performed on male healthy young wistar rats (8–10 weeks old) and weighting between 160 and 200 g. The animals were housed in separated ventilated cages at room temperature (22 ± 3 °C) with a 12 h of light cycle and fed with water and commercial foods. The laser was applied on fractional pulsed carbon dioxide (CO_2) creating microscopic areas of thermal necrosis in the epidermis and dermis of animals. The rats were anesthetized with diethyl ether and exposed to partial-thickness laser skin burn (wound area of 2.2 cm^2), using a CO_2 Fractional Laser System (DSE, Korea) with the following parameters: Density level of 20 and line: 29 × 29, Dot: 0841; Energy level at about 25 MJ and a Depth level of 4.

Four groups of rats were tested for their change in the healing of the induced injury. The groups were as follow (n = 6):

Group 1: *Control group* wounds treated with physiologic serum;
Group 2: wounds treated with standard drug *Cytol basic* cream (Positive control);
Group 3: wounds treated with *CS-TPP NF0* film;
Group 4: wounds treated with *CS-TPP NF4* film.

Each sample of each group, as well as the control group, was tested on six rats and the mean values were recorded. All wounds treatments were carried out daily, using sterilized compresses immediately after burning until the wounds of one of the groups were completely healed.

Wound Healing Contraction

The area contraction of wound, considered as percentage of reduction of the original wound size, was determined as follows:

$$\text{Wounds area contraction} = \frac{A_0 - A_d}{A_0} \times 100$$

where A_0 and A_d were the wound areas at day 0 and at day d, respectively.

The wound surface areas were measured using Autodesk Auto CAD 2015 software application for the designing and drafting. Results were presented as the average values from six rats in the same treated group.

Hydroxyproline Content

Hydroxyproline amount was consisted of the measurement of collagen concentration in rat's tissues. Further, collagen was a constituent of growing cells. Indeed, higher hydroxyproline content indicated a faster rate of wound healing process [31]. The hydroxyproline contents in the wound tissues treated with CS-TPP NF0 and CS-TPP NF4 films, as compared to the control and Cytol basic–treated groups, were determined according to Lee and Tong [32] method.

Histological Study

The wound skin samples from different groups were fixed in a Bouin solution for 24 h, and then transported in 10% of neutral-buffered formalin. The fixed tissues were embedded in paraffin and then sectioned at about 4 µm in thickness. After that, sections were then stained with hematoxylin–eosin and examined under a light microscope (Olympus-CX41).

Statistical Analysis

All experiments were carried out in triplicate, excepting films mechanical properties, where analysis was repeated at least six times, and average values with standard deviation errors were reported. Mean separation and significance were analyzed using the SPSS-software package ver. 13.0 professional edition (SPSS, Inc., Chicago, IL, USA) using ANOVA analysis. With a $p < 0.05$, the differences were considered as significant.

Results and Discussion

Nanoparticle Size Determination

CS-NPs were prepared through simple, convenient, controllable process adding drop wise TPP solution to the CS, the cationic phase, under a gentle magnetic stirring at room temperature, as reported in Fig. 1. When the TPP was added, CS amino groups (pKa = 6.3) were ionically crosslinked through TPP ions (pH of the final suspension was around 5.5). Particles' characteristics such as average particle size and size distribution were conducted using the DLS method. The prepared CS-NPs were characterized by a narrow size of 201.20 ± 0.15 nm. Csaba et al. [33] used ionic gelation method and obtained smaller CS-TPP nanoparticles (at about 93 nm) using chitosan with low molecular weight. Indeed, the difference in the nanoparticles size and their distribution was also attributed to various parameters, such as the MW and deacetylation degree of chitosan, the needles diameter, as well as the concentrations of CS and

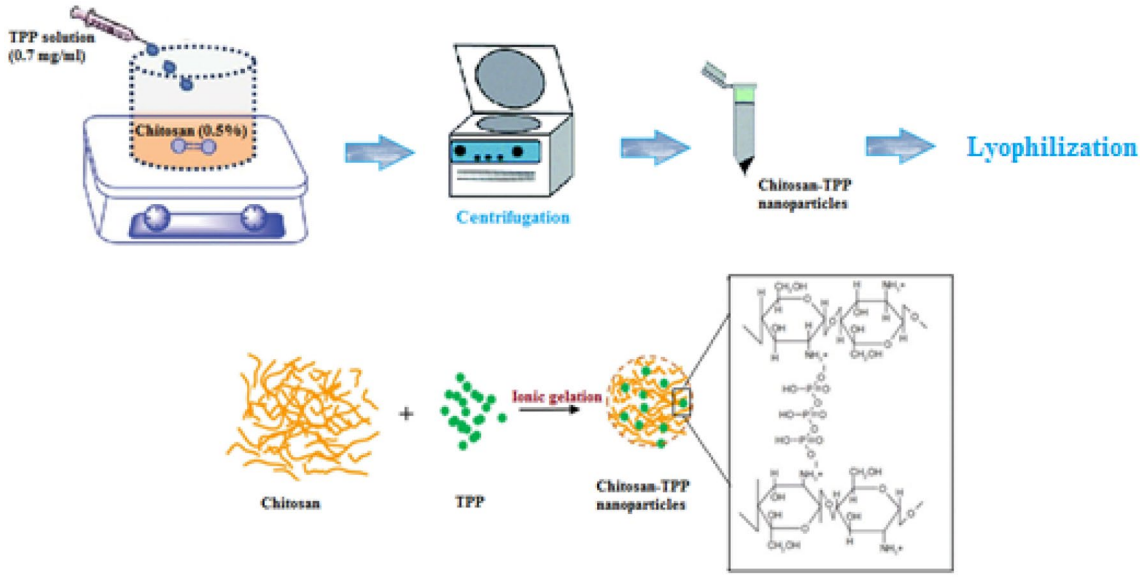

Fig. 1 Schematic representation showing the mechanism of formation of chitosan-sodium tripolyphosphate nanoparticles

TPP used for CS-NPs preparation. Further, other study prepared many batches to optimize CS and TPP concentrations and CS/TPP weight ratios (4/1, 4/2, 4/3 and 4/4) and improved that the size of nanoparticles increased with the increase in the TPP amount from 197 to 393 nm, due to the TPP crosslinking ability, that leads to the formation of larger structures [34]. In addition, they reported that the 4/1 ratio gave the better stability over the time and was probably characterized by a good interaction between the different components. The optimized CS-TPP mass ratio was reported as 5 [35] and 3.75 [36]. Further, Servat-Medina et al. [37] reported that CS concentration of 1 mg/ml, with a CS-TPP polymer ratio of 5 (w/w), a CS-TPP volume ratio of 10, and using mechanical stirring at 7200 rpm, followed by sonication (5 min, 20% amplitude) resulted in the reproducible formation of NPs with an average hydrodynamic diameter of 150 nm. Indeed, the attractive electrostatic interactions between the negatively charged TPP (–OH) and positively charged CS led to the nanoparticles formation by yielding an inter-polyelectrolyte complex [38].

Fish Gelatin Characterization

The structural characterization of fish gelatin was studied using the CP/MAS-NMR spectroscopy. The ^{1}H NMR spectra showed a large peak at about 4.67 ppm (Fig. 2A). Teramoto et al. [39] reported that ^{1}H NMR spectra of fish gelatin presented characteristics peaks at the region of 0–8 ppm, which were probably attributed to the benzene proton of phenylalanine residues.

For the ^{13}C NMR spectrum of fish gelatin, it was observed six signals of the carbon atoms (Fig. 2B). The carbonyl group was observed at around 174.90 ppm. At 43.52 ppm, the band was also attributed to the glycine-α. Indeed, glycine was the most abundant amino acid in collagen and represents about one-third of all amino acid residues. As observed, the peaks at near 25.22 and 29.01 ppm were assigned to proline-γ and proline-β. In fact, glycine and hydroxyproline are the polar amino acids in gelatin. The peaks at 54.86 ppm were attributed to alanine-α and proline-δ. Peak assignments of gelatin were carried out in accordance with earlier reports [40]. In fact, the glycine could easily form hydrogen bonds with the hydroxyl group of chitosan and TPP molecules.

Physicochemical, Structural and Thermal Properties of Films

Film Thickness, Color and Microstructure

CS-NPs were incorporated onto the nanocomposite films based on chitosan and gelatin at different amount (2, 4 and 6 wt%, dry base). Further, the effect of CS-NPs amounts on the thickness of films was also studied and results showed that there is no significant difference with the nanoparticles incorporation, which proved that nanoparticles were well entrapped in the continuous network of polymers matrix (Table 1).

Color was an important index in terms of general appearance and consumer acceptance. Visually, the nanocomposite films were transparent. Table 1 showed the color coordinates (L^*, a^* and b^*) and the total color difference (ΔE) of nanocomposite films. As observed, with the increase in CS-NPs amount (2, 4 and 6%) the redness (a^*) of films decreased slightly. Whereas, no significant changes has been observed

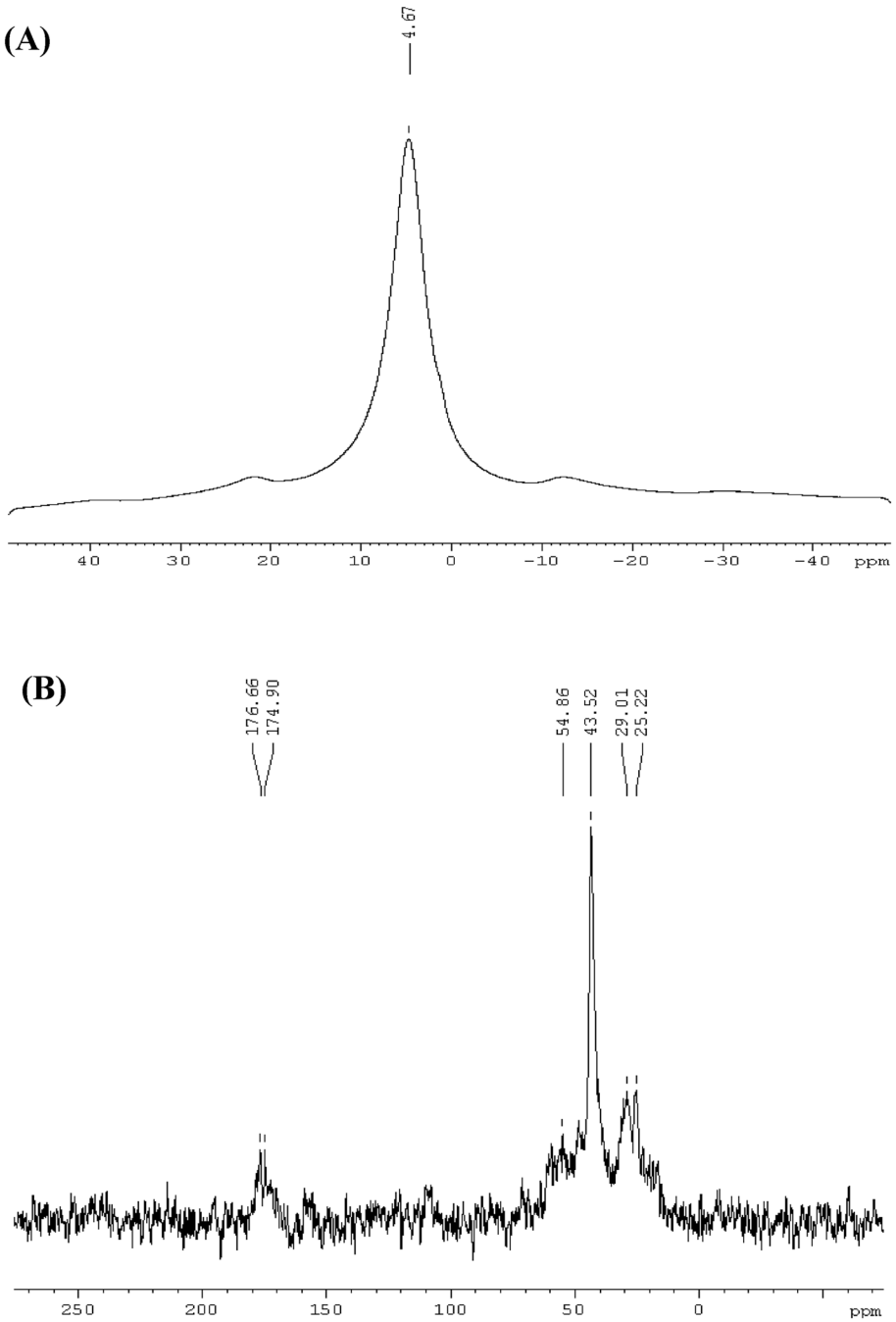

Fig. 2 ^{13}C (**A**) and ^{1}H (**B**) CP/MAS NMR spectra of fish gelatin

in lightness (L^*), while a slight decrease in the yellowness (b^*) values were shown with increasing of the CS-NPs concentrations. Furthermore, for the color difference (ΔE) of CS-TPP NFs, a significant change was observed between the different films formulation which was dependent on the nanoparticles contents.

To better understand the microscopic structure and homogeneity of films and to visualize their surface topography without and with the CS-NPs incorporation, Scanning Electron Microscopy (SEM) was used. As observed in Fig. 3A, CS-TPP NF0 show an homogeneous and smooth surface without any roughness, air bubbles and cracks, which indicated interaction between CS and gelatin components. However, with the CS-NPs incorporation (CS-TPP NF4), the SEM micrograph showed a heterogeneous surface with small aggregates with a compact and tortuous structure. These observations could be attributed to the reduction of interlayer forces between CS-gelatin matrix and nanoparticles.

Table 1 Thickness, EAB, TS, water solubility, swelling degree and color properties of the nanocomposite films

	CS-TPP NF0	CS-TPP NF2	CS-TPP NF4	CS-TPP NF6
Thickness (mm)	0.06 ± 0.01^{a}	0.04 ± 0.02^{a}	0.04 ± 0.01^{a}	0.055 ± 0.01^{a}
EAB (%)	40.27 ± 0.21^{c}	75.63 ± 0.32^{a}	61.52 ± 0.14^{b}	27.90 ± 0.25^{d}
TS (MPa)	36.51 ± 0.25^{c}	36.96 ± 0.14^{c}	40.98 ± 0.20^{b}	44.78 ± 0.03^{a}
Water solubility (%)	45.51 ± 0.15^{a}	44.61 ± 0.43^{b}	41.58 ± 0.54^{c}	34.05 ± 0.14^{d}
Swelling degree (%)	88.20 ± 0.20^{a}	80.32 ± 0.10^{b}	62.30 ± 0.15^{b}	58.49 ± 0.31^{c}
Color parameters				
L*	92.82 ± 0.29^{a}	93.2 ± 1.02^{a}	93.31 ± 0.44^{a}	93.14 ± 0.12^{a}
a*	1.43 ± 0.20^{a}	1.32 ± 0.09^{a}	1.35 ± 0.09^{a}	1.33 ± 0.21^{a}
b*	-1.03 ± 0.13^{c}	-1.59 ± 0.49^{a}	-1.49 ± 0.35^{b}	-1.67 ± 0.17^{a}
ΔE	–	2.76 ± 0.45^{a}	2.67 ± 0.35^{a}	2.73 ± 0.19^{a}

EAB elongation at break, *TS* tensile strength; Values were given as mean ± standard deviation

Means with different superscripts (a–d) within a lines indicate significant difference ($p < 0.05$)

Physicochemical properties were determined at 25 °C and 50% RH

Optical and Structural Characterization

The optical properties of nanocomposite films were studied using UV–Vis spectrophotometer in 200–800 nm range (Fig. 3B). As observed, the CS-NPs incorporation onto nanocomposite films reduced significantly the UV light transmission. Further, the nanoparticles could improve the light barrier property by scattering light and by blocking the light transmission through the nanocomposite films, especially when CS-NPs were dispersed homogeneously in the polymer-gelatin matrix [41].

In order to determine the effect of CS-NPs incorporation on the structural properties of nanocomposite films, two spectroscopic methods, FTIR and XRD were used and the spectra were reported in Fig. 3C and D, respectively. For the FTIR spectra, the broad characteristic peak at 3317 cm^{-1} was also attributed to –OH and –NH stretching of chitosan, as previously observed [42]. In addition, the amide-I and amide-II bands observed at 1658 and 1536 cm^{-1} for CS shifted to 1642 and 1529 cm^{-1} in CS-TPP NF0 spectra, which was also attributed to the possible interaction between CS and gelatin polymers. The sharp peaks observed at 1383 and 1424 cm^{-1} were assigned to the -CH_3 symmetrical deformation mode. The amino groups and C=O stretching vibration of CS observed at 1250 and 1091 cm^{-1} wavelengths were shifted to 1243 and 1089 cm^{-1} in CS-TPP NF0 spectrum, respectively. The observed shifts could be attributed to the hydrogen bonding interactions between gelatin and CS polymer in the composite films.

Jridi et al. [43] reported that the FTIR spectra of films based on gelatin extracted from cuttlefish skin showed characteristic bands at 3272, 3090, 1662, 1546 and 1243 cm^{-1}, which were assigned to the amide-A (–NH stretching), amide-B (asymmetric stretching vibration of -CH and NH_3^+), amide-I, amide-II and amide-III (vibrations in plane of –CN and –NH groups of bound amide or vibrations of CH_2 groups of glycine), respectively. Further, for the CS-TPP NF0 spectra, the amide-A and amide-III peaks did not show any shifts, as compared to gelatin spectra. However, the amide-I and amide-II shifted to lower wavelengths and appeared at near 1642 and 1529 cm^{-1}. The observed differences may be attributed to the alteration of secondary structure of gelatin polypeptide caused by the addition of CS polymer [44].

For the films enriched with nanoparticles, it was observed a remarkable shift of many peaks, as compared to control film. Indeed, the amide-I shifted from 1642 to 1618 cm^{-1} for CS-TPP NF2, while it disappeared for the other nanocomposite films, implying the possible molecular interaction between CS-gelatin matrix with CS-NPs. In addition, the amide-II band shifted to 1512 and 1507 for CS-TPP NF2 and CS-TPP NF6, respectively, with a significant increase in their intensity. At 1401 cm^{-1}, the symmetrical deformation mode of -CH_3 showed a slight shift (especially observed for CS-TPP NF6) with the CS-NPs incorporation. The amide-III (1240 cm^{-1}) band did not show any shift with the nanoparticles addition, while a decrease in intensity of peak was observed, revealing the possible interaction between CS-gelatin matrices with nanoparticles. Furthermore, the observed shifts and the disappearance of the amide-A (3268 cm^{-1}) in CS-TPP NF0 spectrum indicated the possible decrease of gelatin hydrophilicity, which could be attributed to the hydrogen bond between the free –OH group of gelatin and CS-NPs [45].

It can be concluded that the appearing of newly peaks and a shift in various peaks may occur due to the formation of hydrogen bonding between CS-NPs and CS-gelatin matrix in nanocomposite films. These interactions lead to the good compatibility between the different components, inducing the enhancement of mechanical and physicochemical properties of nanocomposite films.

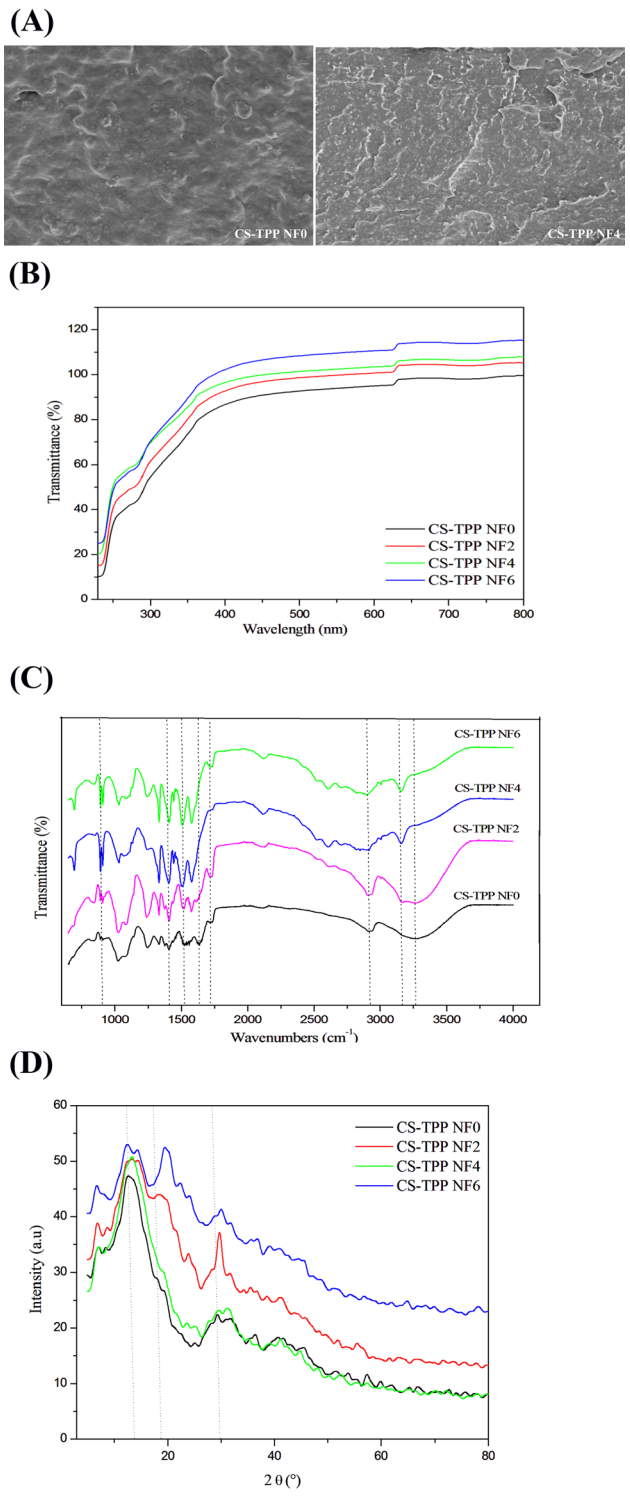

Fig. 3 High resolution Scanning Electron Microscopy micrographs of CS-TPP NF0 and CS-TPP NF4 (**A**), UV–Visible absorption (**B**), FTIR (**C**) and XRD (**D**) spectra of nanocomposite films

The XRD spectroscopy was one of the most common methods used to study the miscibility between the different components of the composite films, as well as the crystalline level determination. For the CS powder, the XRD pattern showed two diffraction peaks at $2\theta = 10.05°$ and 19.86° corresponding to the respective equatorial [0 2 0] and [1 1 0] of the microcrystalline reflections of chitosan [46]. The XRD pattern of CS-TPP NF0 exhibited three main peaks at $2\ \theta = 12.49°$, 18.06° and 29.18° corresponding to [1 0 1], [1 0 $\bar{1}$] and [0 0 2] atomic planes of CS-gelatin matrix, respectively (Fig. 3D). The CS-NPs incorporation in different contents exhibited significant changes in the XRD patterns of nanocomposite films. Furthermore, it was observed a shift in the characteristic peaks at around $2\ \theta = 12.6°$, 14.6°, 19.5° and 30.11°, which was also attributed to the possible alteration of the film structure. These observations were also attributed to changes in the crystalline structure of films produced by chemical interactions between CS-NPs and chitosan–gelatin matrix [47].

Changes in XRD patterns suggested the ionic interactions between CS-NPs, CS-gelatin matrix, which leads to the change in the crystallinity of nanocomposite films. After the CS-NPs crosslinking, the crystalline peaks of the nanocomposite films showed change in the morphology which proved the good miscibility of different components. With nanoparticles incorporation onto films, the crystallinity indices showed an increase to 37.8% and 49.1% for CS-TPP NF0 and CS-TPP NF6, respectively. Results were in line with Rubentheren et al. [48] study, which reported an increase in intensity of the major peak in the XRD patterns of chitosan nanocomposites reinforced with chitin whiskers and tannic acid, used as a crosslinker. Indeed, the deformation of crystal structure of nanocomposite films could be explained by the breaking of hydrogen bonds between $–NH_2$ and –OH groups of CS resulting from ionic crosslinking with TPP.

Water Solubility and Swelling Degree

Water solubility was an important property of films used as protective layers in food packaging and in biomedical materials. Indeed, the target applications required a low water solubility of materials to enhance the products integrity and water resistance. As presented in Table 1, CS-TPP NF0 film showed moderate water solubility at about 45.51%, comparable to those reported by Jridi et al. [43] for composite films based on skin cuttlefish (*Sepia officinalis*) gelatin and shrimp chitosan (40.36%).

A pH between 5.5 and 6.0 promoted efficacy the formation of polyelectrolyte complex between CS and gelatin. Indeed, a pH higher than the isoelectric point of the gelatin ($Ip = 4.5–5.2$) gives it a negative overall charge and below the pKa of chitosan amine group ($pKa = 6.2–6.5$). Further, the positive charge of CS induced the possible interactions between the two biopolymers. Indeed, the CS-TPP NF0 film was characterized by lower water solubility, as compared to gelatin film (75%), but slightly more soluble than chitosan

film (33.28%). Taravel and Domard [49] reported a similar result and suggested a possible interaction by electrostatic forces and hydrogen bonding between the amino groups of CS and the carboxyl groups of gelatin.

The CS-NPs incorporation induced a significant decrease in the water solubility, where CS-TPP NF0 was the less resistant film (45.51%), as compared to nanocomposite films. Results were comparable to those reported by De Moura et al. [50] study, which showed that CS-NPs addition reduced significantly the water solubility of the methyl cellulose films. Indeed, the decrease in water solubility was also attributed to the formation of polyelectrolyte complexes in CS-gelatin matrix, through negatively charged side-chain groups in gelatin (carboxylate groups) and the positive charge of ammonium groups of CS polymer with nanoparticles via electrostatic interactions [51].

Furthermore, as observed in Table 1, CS-NPs incorporation onto nanocomposite films induced a significant ($p < 0.05$) decrease in the swelling degree between CS-TPP NF0 (88.20%) to attain 58.49% for CS-TPP NF6. Further, the crystalline property of CS-NPs could acts as a hydrophobic barrier that prevents water molecules from getting into CS-gelatin matrix. This improved the cohesiveness of nanocomposite films and a decrease in their water sensibility. According to Chang et al. [52], the addition of CS-NPs produced a tortuous path that hinders the penetration of water molecules through the film matrix. Based on the above results, it can be inferred the strong interactions through hydrogen bonding between the negatively charged side-chain groups (carboxylate groups) and the amino and hydroxyl groups of CS-NPs, as demonstrated previously by FTIR study.

Mechanical Properties

The effects of CS-NPs incorporation at different amounts on the mechanical properties of nanocomposite films were also studied and results were given in Table 1. As observed, the tensile strength (TS) of CS-TPP NF0 was the lowest (36.51 MPa) amongst the nanocomposite films, and the incorporation of CS-NPs enhanced significantly the TS from 36.96 to 44.78 MPa (CS-TPP NF6). Nanoparticles could serve as a junction that improved the tensile strength and increased the flexibility of chitosan molecules. Therefore, 6 wt% of CS-NPs were the appropriate content to the TS of the nanocomposite films. The nanoparticles acted as a reinforcing agent in plasticized-chitosan matrices and this behavior was explained by the electrostatic interactions between nanoparticles with biopolymeric matrix. Results were in line with Chang et al. [52] study which reported that CS-TPP nanoparticles improved significantly the mechanical and barrier properties of composite films.

With the nanoparticles incorporation, EAB of films increased significantly from 40.27 to 75.63% for CS-TPP NF0 and CS-TPP NF2, respectively. However, increase of nanoparticles amount up to 2% (wt. %) reduced significantly ($p < 0.05$) the EAB of nanocomposite films from 61.52 to 27.9% for CS-TPP NF4 and CS-TPP NF6, respectively. Indeed, the EAB decreases could be attributed to the aggregation of CS nanoparticles after a certain concentration was reached, which could disturbed the structural integrity of polymer-gelatin matrix and induce preferential breaking zones. De Moura et al. [53] showed that CS-TPP nanoparticles incorporation onto hydroxypropyl methylcellulose, with a nanoparticle size of about 85 nm, induced the EAB increases from 8.1 to 11.1% and the elastic modulus from 900 to 1264 MPa, as compared to control film. Further, they observed an increase of the TS from 28.3 to 62.6 MPa of films after nanoparticles incorporation.

Moreover, Martelli et al. [54] reported that the incorporation of chitosan nanoparticles (88.78 nm) at a concentration of 0.2% of dry weight improved noticeably the mechanical properties and elasticity of composite films. Indeed, the mechanical properties improvement of films enriched with CS-NPs could be attributed to different factors, such as the homogeneously dispersed nanoparticles, the presence of interactions between nanoparticles and CS-gelatin matrix and an effective load transfer from polymer chains to the nanoparticles.

Thermo-Dynamical Properties

To further explore the interactions between CS-NPs and CS-gelatin matrix, the nanocomposite films were characterized by TGA in temperature range of 25–600 °C. Thermal stability, decomposition temperature and residual mass of CS-TPP NFs were examined by TGA technique. The typical TGA curves of CS-TPP NFs were reported in Fig. 4A. The thermal curves clearly exhibited the thermal decomposition patterns. Table 2 reports the maximum degradation rate temperature (T*d*), the different weight loss steps (ΔW) and the corresponding final residual mass of CS-TPP NFs. As observed, CS-TPP NF0 showed four step weight losses of 9.0, 5.9, 43.5 and 11.1% in temperature range of 25–600 °C with a final residual mass of 16.4%. In addition, CS-TPP NF2 showed four mass-loss steps. Indeed, the initial thermal decomposition in the temperature ranges of 25–170 °C was mainly due to the evaporation of water (adsorbed and bound water) retained in the films, whereas, the second thermal event (from 170 to 250 °C) was also attributed to the evaporation of glycerol, used as a plasticizer agent. The third weight loss was observed between 250 and 400 °C, corresponding to the degradation of saccharide rings, depolymerization, and decomposition (oxidative and thermal) of the CS-TPP NFs matrix (*T*d: 314 °C). The last weight loss step observed from 400 to 600 °C (13.7%) with a residual mass

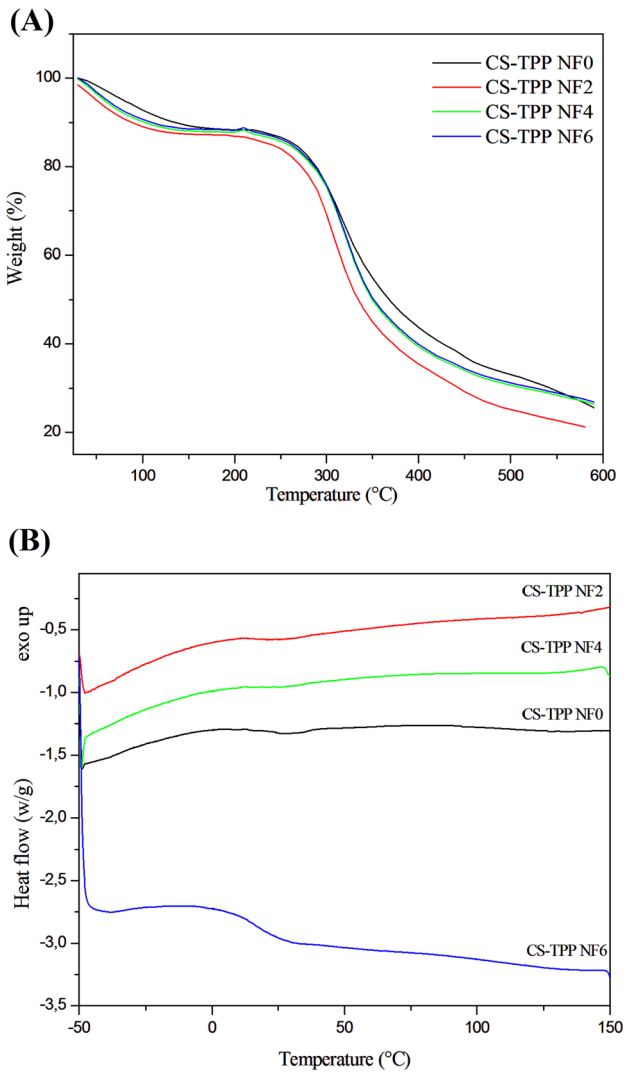

Fig. 4 Thermogravimetric analysis: curves showing TGA (**A**) and thermal stability by DSC analysis (**B**) of nanocomposite films

of 29.0% corresponds to final degradation of both gelatin and chitosan polymers. This mass reduction corresponds to the degradation of CS-NPs (*T*d of CS cross-linked with TPP or TPP) [55]. Further, The T*d* exhibited a lower increase with the CS-NPs content from 2 to 6 wt%. It can be deduced that CS-TPP NFs were decomposed at higher temperature than those without nanoparticles, reflecting the thermal stability improvement of nanocomposite films.

The thermal properties of composite films were assessed by the DSC analysis (Fig. 4B) in order to determine the glass transition temperature (*T*g) from the second heating cycle (Table 2). CS-TPP NFs were characterized by a *T*g at about 18–19 °C. Further, *T*g values could be attributed to the characteristics of gelatin and chitosan used for the nanocomposite films preparation, such as the molecular weight and deacetylation degree of CS, as well as the amino-acids composition and molecular weight of gelatin. Indeed, the presence of one *T*g value in the DSC thermograms can be interpreted by the complete miscibility of the different compounds in the nanocomposite films. Results were in line with those of Hosseini et al. [56], which reported that CS and gelatin were characterized by a good miscibility and could form a wide range of blend films, in which new hydrogen bonding networks appeared. Further, they showed a *T*g value of 56 °C for gelatin-chitosan (G60/CS40) composite films with an EAB and TS of 25.30% and 16.60 MPa, respectively.

As can be seen, *T*g did not show any difference with the CS-NPs incorporation, as compared to the CS-TPP NF0 and the appearance of one *T*g revealed the compatibility between the different components constituting the nanocomposite films. This finding may be attributed to the intermolecular hydrogen bonds between nanoparticles, the hydroxyl and amine group's presents in chitosan and gelatin bio-polymers. This fact provided additional evidence that the CS-NPs incorporated into nanocomposite films did not affect their crystalline structure, which was deduced by the unmodified *T*g values.

DMA is a technique that is helpful for estimating the increase in stiffness of the composite films induced by nanoparticles incorporation. As shown in Fig. 5A, the storage modulus (*E′*) of nanocomposite films increased with the CS-NPs incorporation. This improvement was likely due to the interaction between the nanoparticles with CS-gelatin matrix. Figure 5B and C showed the curves for the loss modulus (*E″*) and Tan δ as a function of temperature for

Table 2 Determination of weight loss percents (ΔW), decomposition temperature (*Td*), residual mass and glass transition temperature (*Tg*) of the CS-TPP NFs

Samples	ΔW1 (%)	ΔW2 (%)	ΔW3 (%)	ΔW4 (%)	*Td* (°C)	Residual mass (%)	*Tg* (°C)
CS-TPP NF0	9.0	5.9	43.5	11.1	315	16.4	18
CS-TPP NF2	10.6	7.7	38.8	13.7	314	29.0	19
CS-TPP NF4	8.3	4.3	37.1	8.2	319	41.7	18
CS-TPP NF6	7.8	5.4	35.7	7.9	319	40.0	19

ΔW represents the weight losses, *Td* the decomposition temperature, *Residual mass* the residual mass of samples at 600 °C, *Tg* the glass transition temperature

The average relative error of DSC and TGA data was lower than 10%

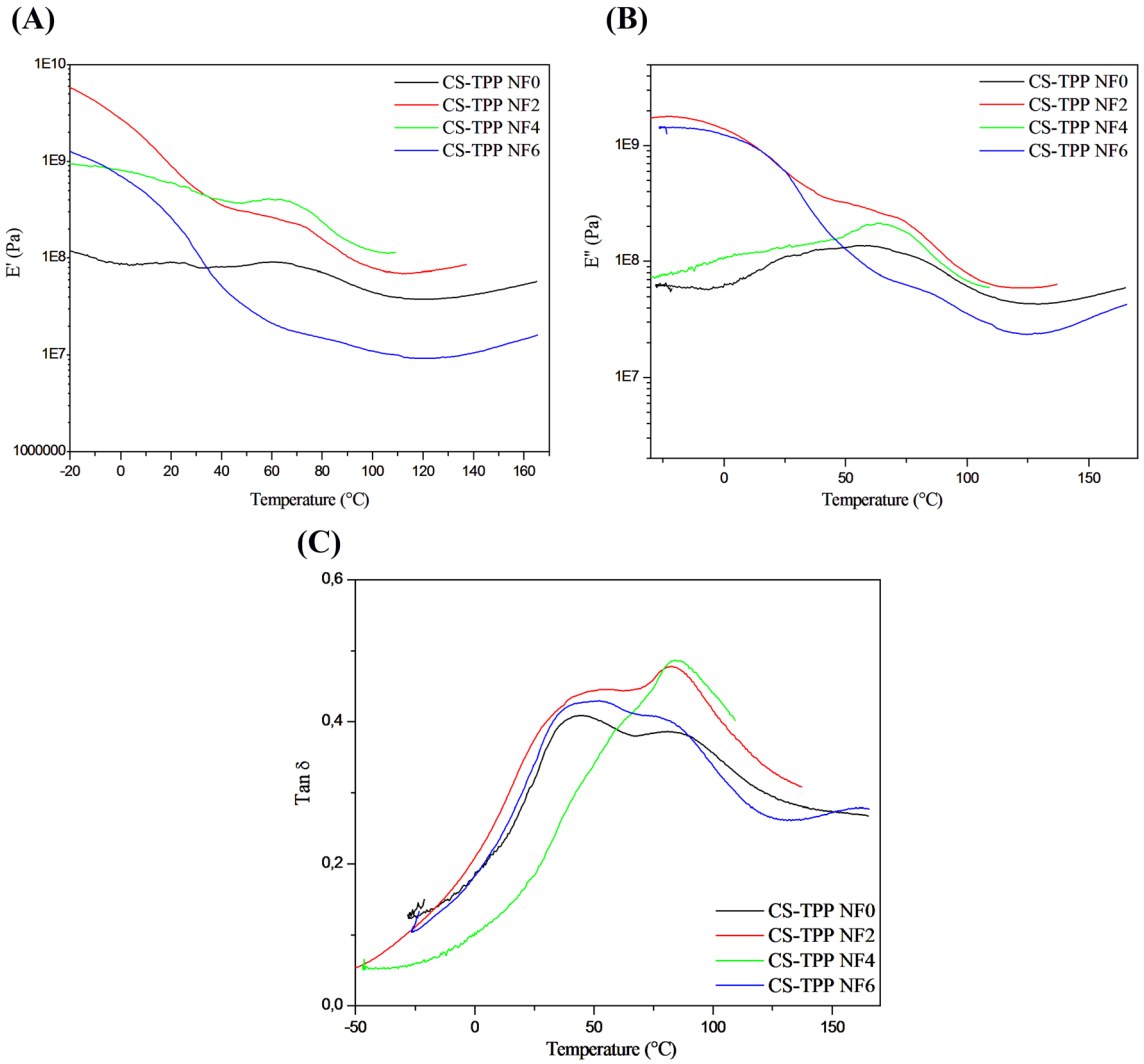

Fig. 5 Evolution of the storage tensile modulus *E′* (**A**), loss tensile modulus E″ (**B**) and Tan δ (**C**) versus temperature at 1 Hz of the nanocomposite films

CS-TPP NFs. Tan δ curves exhibits two broad relaxations at around 45 °C and 100 °C. Indeed, the first and the second peaks were also attributed to the *T*g and decomposition of CS-gelatin matrix, so the loss of the crystalline zone.

The loss factor was sensitive to the molecular motion and peak represented the glass transition temperature (*T*g). In the DMA spectra of the nanocomposite films, the glass transition shifted to a higher temperature, indicating that CS-NPs improved the intermolecular interaction between CS and gelatin and could acted as a functioning like a junction, bringing adjacent chains of CS and reduced the free volume in the matrix. Results were also confirmed by DSC analysis. Further, Chang et al. [52] reported an improvement effect on the tensile strength, storage modulus and *T*g of CS-TPP nanoparticles incorporated onto starch composites films.

Wettability and Surface Properties

The surface hydrophobicity of nanocomposite films was evaluated via measuring the contact angle (θ) of different solvents (water, ethylene glycol and diiodomethane) upon the film surface using the sessile drop method. Further, contact angle measurement was one of the key properties of foods packaging as well as the biomedical materials, which was usually used as an important indicator for the hydrophobic/hydrophilic properties of films surface. Practically, a contact angle higher than 90° ($\cos\theta < 1$) represents a hydrophobic surface, whereas a contact angle lower than 60° ($\cos\theta > 0.5$) implies a hydrophilic surface [30].

The water contact angle (WCA) values measured for control CS-gelatin (CS-TPPNF0) film and films enriched with nanoparticles at different time (0, 60 and 120 s) was

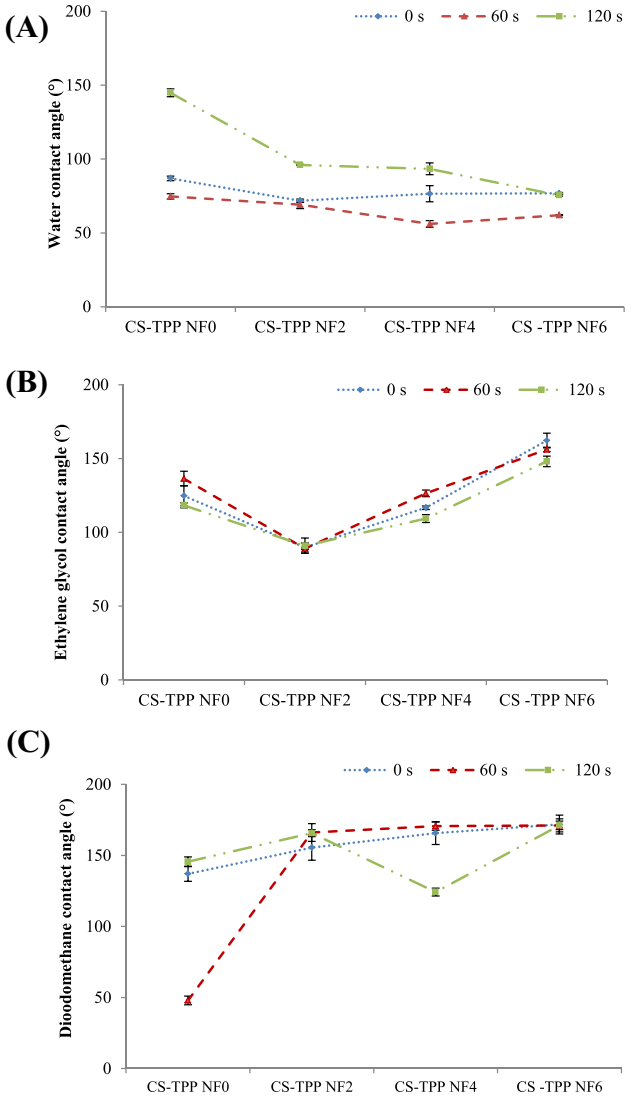

Fig. 6 Contact angle for the different films, as a function of time, by using water (**A**), Ethylene glycol (**B**) and Diiodomethane (**C**) solvents

displayed in Fig. 6A. Control film exhibited an initial WCA value of 86.9° at t = 0 s. After CS-NPs incorporation, WCA decreased to 75.4° for CS-TPP NF6. Generally, films having the highest WCA values exhibited a higher surface hydrophobicity, thus having better potential to overcome the limitation of hygroscopicity [57]. Further, Rehman et al. [58] reported that chitosan–gelatin coatings were characterized by a hydrophobic character with a high contact angle of 120°.

Results were in agreement with previous study, which showed that the gelatin incorporation onto chitosan matrix increased the hydrophobicity, due to its hydrophilic character [59]. Indeed, results could be attributed to the formation of polyelectrolyte complex due to the possible interactions between the positive charges of chitosan and gelatin molecules. This polyelectrolyte complex may decrease the charge

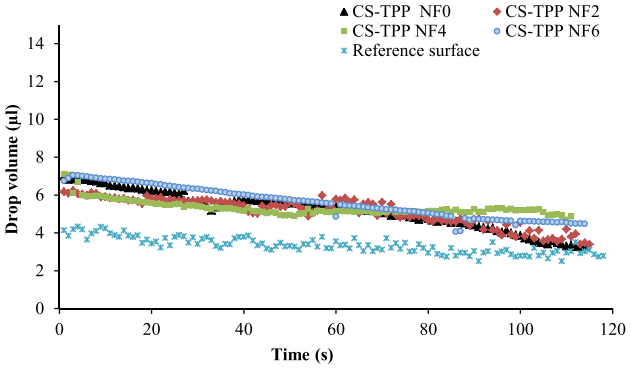

Fig. 7 Kinetics of wetting of the nanocomposite films as a function of time using water droplets, as compared to reference surface (Aluminum foil)

density on the surface, which decrease the polarity of the chitosan complex and increased its hydrophobic character [60].

CS-TPP NF0 was characterized by an important increase in the WCA from 86.9 to 144.87° in time range of 0–120 s, which could be attributed to the increase in surface hydrophobicity of films. For CS-TPP NF2 and CS-TPP NF4, an increase in the WCA values from 69.14° and 76.53° (t = 0 s) to 96.01° and 93.40° after 120 s, respectively, was observed.

Two other solvents (ethylene glycol and diiodomethane) were also used for the surface and wettability parameters determination. Figure 6B and C showed the change of the contact angle with time for CS-TPP NFs without and with nanoparticles incorporation. Further, CS-TPP NF2 did not show any significant difference in CA at 0, 60 and 120 s (≈ 89 and 155°) for ethylene glycol and diiodomethane, respectively. On the contrary, a significant decrease in the CA for the other nanocomposite films, which was dependent on time and film composition.

The film wettability was an important factor to consider materials for biomedical applications. It was also investigated by examining the behavior of water droplets deposited on the film surface as a function of time. Variation of droplets volume were also determined and results showed that the volume of water droplets deposited on the surface of CS-TPP NF0 decreased slowly as a function of time (0–120 s). However there are no differences between the nanocomposite films with different nanoparticles amounts (Fig. 7). As compared to the reference surface (aluminum foil), it was observed a low slope variation, which was also attributed to a slight absorption by the nanocomposite film. Indeed, according to Karbowiak et al. [61] method, the water absorption flux (F_{abs}) was determined. Results showed that the F_{abs} of films without nanoparticles was 0.5 10^{-2} L/m^2 s, whereas, for the enriched films with NPs, it was ranged from 0.15 to 0.25 10^{-2} L/m^2 s. This behavior could be related to the dispersive component of the surface free energy.

Table 3 Surface properties of nanocomposite films: surface free energy, polar and dispersive components as a function of time (0, 60 and 120 s)

Time (s)	Films	Polar component (γ_S^P) (mN/m)	Dispersive component (γ_S^D) (mN/m)	Surface free energy (γs) (mN/m)
0	CS-TPP F0	21.93 ± 1.94^{d}	0.05 ± 0.02^{d}	21.97 ± 1.93^{c}
	CS-TPP F2	27.34 ± 0.30^{c}	4.79 ± 0.03^{a}	32.13 ± 0.34^{b}
	CS-TPP F4	42.33 ± 0.81^{a}	1.25 ± 0.07^{c}	43.25 ± 1.40^{a}
	CS-TPP F6	32.63 ± 0.30^{b}	3.14 ± 1.54^{b}	35.77 ± 1.45^{b}
60	CS-TPP F0	32.38 ± 2.73^{d}	1.91 ± 0.69^{b}	34.30 ± 2.14^{d}
	CS-TPP F2	44.69 ± 1.75^{c}	0.10 ± 0.01^{c}	44.70 ± 1.75^{c}
	CS-TPP F4	65.69 ± 1.28^{a}	4.04 ± 0.08^{a}	69.74 ± 1.21^{a}
	CS-TPP F6	56.30 ± 0.62^{b}	2.07 ± 1.43^{b}	58.37 ± 2.02^{b}
120	CS-TPP F0	0.74 ± 0.86^{c}	0.69 ± 0.14^{b}	1.43 ± 0.88^{c}
	CS-TPP F2	19.93 ± 0.06^{b}	0.11 ± 0.03^{c}	20.04 ± 0.05^{b}
	CS-TPP F4	21.47 ± 0.68^{b}	0.48 ± 0.51^{b}	21.95 ± 0.80^{b}
	CS-TPP F6	33.47 ± 3.20^{a}	3.38 ± 2.01^{a}	36.85 ± 0.77^{a}

Values were given as mean ± standard deviation. Means with different superscripts (a–d) within a column at the same time (0, 60 or 120 s) indicated a significant difference ($p < 0.05$)

In addition, based on the behavior of nanocomposite films against the different solvents and by using the sessile drop method, the surface energy was calculated as shown in Table 3. For the control film (CS-TPP NF0), the values of the polar (γ_S^P) and dispersive components (γ_S^D) were initially about 0.05 and 21.93 mN/m, respectively. However, after the CS-NPs incorporation and especially for CS-TPP NF2, both components increased significantly to 4.79 and 27.34 mN/m, respectively.

These observations were also observed for the surface free energy (γ_S). The highest polar component (42.33 mN/m) and surface free energy (43.25 mN/m) were recorded for CS-TPP NF4, which may be due to its hydrophilic property. Further, CS-TPP NF2 showed the highest dispersive component, as compared to the other nanocomposite films.

The polar and dispersive components, as well as the surface free energy showed initially an increase followed by a decrease after 60 and 120 s, respectively (Table 3). Results showed that the wetting tension was affected by the nanoparticles incorporation onto the nanocomposite films. In fact, the wettability of films could be affected by the possible interactions between the different components such as chitosan, gelatin and nanoparticles, which were previously confirmed by FTIR spectra. Therefore, CS-NPs addition increases the hydrophilicity of CS-gelatin composite films as proved by the contact angle values variation and the surface free energy parameters.

Bioactive Potentials of Nanocomposite Films

In Vitro Antioxidant Assay

The antioxidant activity of the nanocomposite films was assessed via different tests: DPPH radical-scavenging activity, ferric-reducing power, β-carotene bleaching assay and ABTS-scavenging ability.

DPPH, a stable free radical, was widely used for the determination of free radical-scavenging efficiencies of different materials by determining the decrease of DPPH-radical absorbance at 517 nm, caused by the scavenging of the hydroxyl radical through hydrogen atom or an electron donation. The DPPH scavenging ability of nanocomposite films was carried out and results showed that the CS-TPP NFs exhibited important antioxidant activity against DPPH, which was dependent on nanoparticles amount (Table 4). Also, composite films enriched with 6 wt% of nanoparticles showed a noticeable effect by inhibiting radical formation

Table 4 Antioxidant activities of CS-TPP nanocomposite films

Antioxidant activities	CS-TPP NF0	CS-TPP NF2	CS-TPP NF4	CS-TPP NF6
DPPH-scavenging ability (%)	49.20 ± 0.20^{d}	52.92 ± 0.18^{c}	61.67 ± 0.23^{b}	69.41 ± 0.90^{a}
Ferric reducing power ($OD_{700\ nm}$)	0.10 ± 0.25^{c}	0.11 ± 0.25^{c}	0.18 ± 0.05^{b}	0.23 ± 0.15^{a}
β-carotene bleaching activity (%)	43.93 ± 0.30^{d}	55.78 ± 0.10^{c}	70.68 ± 0.40^{b}	72.86 ± 0.50^{a}
ABTS-scavenging activity (%)	36.06 ± 0.24^{c}	36.75 ± 0.25^{c}	45.87 ± 0.53^{b}	50.54 ± 0.12^{a}

Values were given as mean ± standard deviation. Means with different superscripts (a–d) within a same line indicate significant difference ($p < 0.05$)

(at about 69.41%), which was higher than CS-TPP NF2 (52.92%) and CS-TPP NF4 (61.67%). Zhan et al. [62] reported that TPP films loaded with silver nanoparticles showed a high DPPH radical scavenging activity (80%).

Likewise, β-carotene bleaching ability of nanocomposite films was also studied. Results showed that nanocomposite films prevent bleaching of β-carotene which increased with CS-NPs amount, which acted as electron donors and chelating agents. Further, CS-TPP NF6 showed the highest β-carotene bleaching activity (72.86%), as compared to the other nanocomposite films. Melo et al. [63] reported that the use of coatings based on chitosan nanoparticles obtained by ionic gelation was effective to delay the ripening process of grapes at 25 °C for 12 days. Indeed, chitosan-nanoparticles coatings blocked the pores present in the grape surface, thus prevented the moisture loss and controlling the respiration process. The nanocomposite films could acting as a semi permeable barrier around the fruits and could modify the internal atmosphere by decreasing the O_2 gas and increase in the CO_2, and could decrease the ethylene production.

The ABTS radical cation decolorization assay was a widely used method for the assessment of the antioxidant activity of various compounds and edible films. In the present study, CS-TPP NF6 enriched with 6% of CS-NPs showed the highest ABTS scavenging values (50.54%), as compared to control film CS-TPP NF0 (36.06%). Further, nanocomposite films exhibited poor ferric reducing power (OD_{700nm} = 0.1–0.23), which could be attributed to the lower solubility of the films.

Interestingly, the CS-NPs incorporation onto the nanocomposite films matrices improved their antioxidant properties. All of these properties of produced composite films give them the opportunity to be successfully used in food industries as bioactive packaging and as a wound healing agent.

Antibacterial Activity of Nanocomposite Films

The antimicrobial activity of CS-TPP NFs containing different content of CS-NPs was evaluated against *B. cereus*, *S. aureus*, *M. luteus*, *E. coli*, *K. pneumoniae*, *S. enterica*, *S. typhimurium and Enterobacter sp.* bacteria strains via the agar disc diffusion assay (Table 5). The control film (CS-TPP NF0) showed an antibacterial effect against all tested bacteria strains with an inhibition zone diameter in the range of 7–12 mm after 18 h of incubation at 37 °C. The antibacterial activity of CS-TPP NFs was related to the composite films composition and especially the CS-NPs amounts. Results indicated that nanocomposite films have significantly higher antimicrobial activity on all Gram-positive bacteria and Gram-negative bacteria and especially against *B. cereus*, *S. aureus*, *Enterobacter* sp. and *K. pneumoniae* than those without nanoparticles (CS-TPP NF0).

In addition, nanocomposite film with the highest amount of nanoparticles (CS-TPP NF6) showed the largest inhibition zone against *Enterobacter sp*., *E. coli* and *M. luteus* (15 and 14 mm). However, CS-NPs content (2–6 wt%) did not show any significant effect on antimicrobial activity against *E. coli* (7 mm). The bactericidal action of nanoparticles incorporated onto the nanocomposite films might be exerted through different mechanisms. Indeed, the main mechanism induces the generation of reactive oxygen species and oxidative stress. Another possible mechanism for the antimicrobial property was the smaller sizes of the CS-NPs that could diffuse through the bacterial membrane by possible electrostatic interactions, which caused the bacterial growth inhibition as well as the cellular death. The antimicrobial activity of CS-NPs could be attributed to their crystal structure, size and shape, high surface area to volume ratio [64], as well as the small and compact particle size of nanoparticles and their high surface charge [65].

Table 5 Antimicrobial activity of the nanocomposite films against Gram positive and Gram negative bacteria

Indicator organisms	Inhibition zone diameter (mm)			
	CS-TPP NF0	CS-TPP NF2	CS-TPP NF4	CS-TPP NF6
Gram (+)				
B. cereus	9.5 ± 0.5^{d}	12.0 ± 0.5^{c}	13.5 ± 0.5^{b}	14.0 ± 0.5^{a}
S. aureus	9.0 ± 0.5^{c}	8.5 ± 0.5^{c}	11.5 ± 0.6^{b}	12.5 ± 0.5^{a}
M. luteus	10.5 ± 0.5^{c}	12.5 ± 0.6^{b}	13.0 ± 0.5^{b}	14.0 ± 0.5^{a}
Gram (−)				
S. enterica	12.0 ± 0.25^{b}	12.0 ± 0.5^{b}	12.5 ± 0.5^{a}	13.0 ± 0.5^{a}
E. coli	7.0 ± 0.5^{b}	7.0 ± 1.5^{a}	7.0 ± 0.5^{b}	7.0 ± 0.5^{b}
Enterobacter sp.	10.0 ± 1.5^{c}	13.0 ± 0.5^{b}	13.0 ± 0.5^{b}	15.0 ± 0.5^{a}
S. typhimurium	9.0 ± 0.5^{c}	9.0 ± 0.5^{b}	10.0 ± 0.5^{b}	10.0 ± 1.2^{a}
K. pneumoniae	7.5 ± 0.5^{c}	9.0 ± 0.5^{c}	13.0 ± 0.7^{a}	13.0 ± 0.5^{a}

Values were given as mean ± standard deviation. Gram (+): Gram positive bacteria. Gram (−): Gram negative bacteria. Means with different superscripts (a–d) within a line indicate significant difference ($p < 0.05$)

In Vivo Wound Healing Study

Chromatic Study

The wound healing potency of CS-TPP NF0 and CS-TPP NF4 was evaluated on male wistar rats subsequently by the laser burn induction. The wound cicatrization process was assessed based on chromatic study evaluating the regular changes in wound aspect and color during the different healing phases. Wound photographs of a representative rat from each group were taken after 1, 3, 5, 7 and 8 days of treatment (Fig. 8). By the laser burn induction, dark red color reflecting the burn zone was observed in all groups in the first day of treatment. As observed, on the third day, the burns have a brown color which was due to the scab formation. Nevertheless, on 5th day a dark red coloration was observed on the following days in the CS-TPP NF0 and especially CS-TPP NF4 treated groups, which announce the initiation of wound healing process. After 7th days, a healthy skin was observed especially for the treated groups suggesting the wound site reparation and the granulation tissue development. Nonetheless, the untreated (physiological serum) group and Cytol basic-treated group showed, at the end of the experimentation, an open wound with red colored tissues. Shao et al. [22] reported that silver nanoparticles incorporated onto chitosan-based membranes promote the wound healing process healed in compared to control group, which might be due to a synergistic effect of both chitosan and silver nanoparticles.

Wound Closure and Epithelialization Evaluation

As observed in photographs (Fig. 9), each group revealed different rates of wound contraction. The treated groups with CS-TPP NF0 and CS-TPP NF4 displayed a significant wound

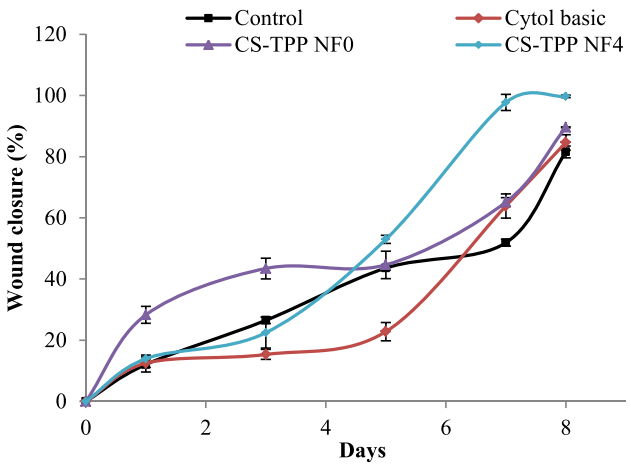

Fig. 9 Effects of nanocomposite films on wound's evolution: Reduction of wound contraction diameter (0–8 days). Each data point represents the mean ± SD of six rats

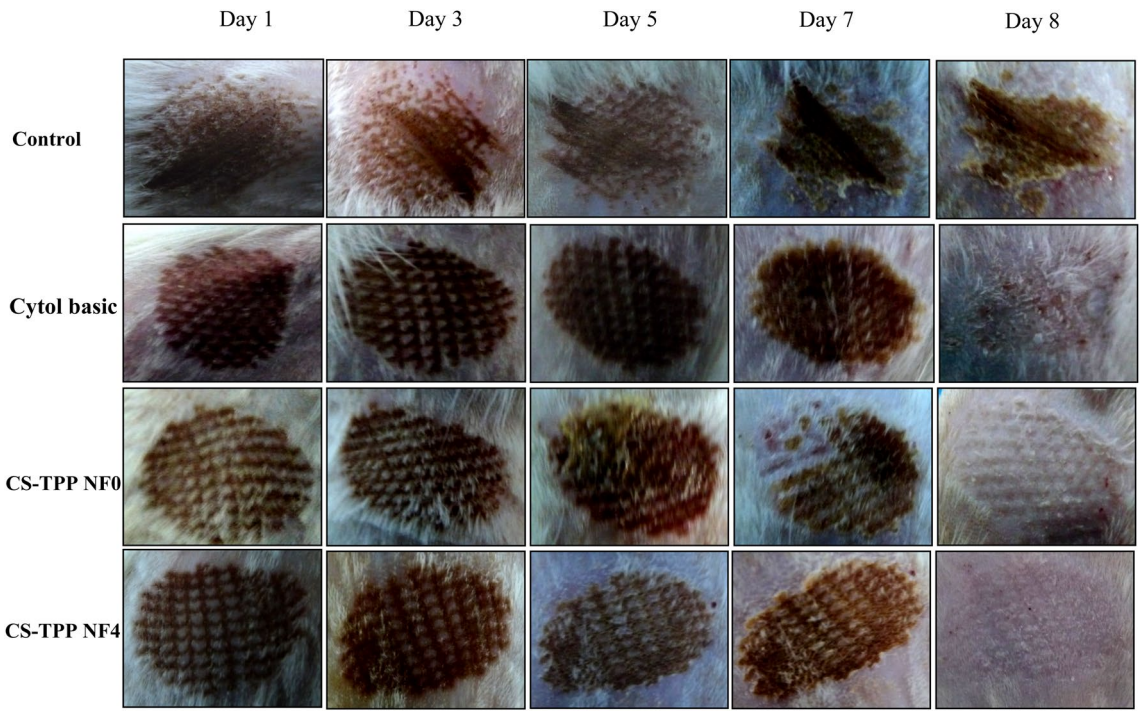

Fig. 8 Representative photographs of excised wounds of rats treated with physiological serum, Cytol basic, CS-TPP NF0 and CS-TPP NF4. The photographs of the wound were observed on 1, 3, 5, 7 and 8 days. Each data point represents the mean ± SD of six rats

healing progression, compared to the others groups. Approximately 50% of the wounds contraction was achieved on days 5, 6, 7 and 7 for CS-TPP NF4, CS-TPP NF0, "Cytol basic" and control (untreated) groups, respectively. All wounds showed a reduction in size over time, regardless of the group to which they belonged. However, the group treated with the CS-TPP NF0 and CS-TPP NF4 films showed full wound closure in the animals (89.58 and 100%, respectively) at the 8th day. Although for the untreated and "Cytol basic" groups, it was 81.55% and 84.63%, respectively. This suggests that treatment with the nanocomposite films enhanced the wound healing, as compared to the other groups. Wang et al. [66] reported that the rate of wound closure increased to 85.6% within 7 days and 98.7% within 14 days of treatment with hydrogels based on chitosan nanoparticles. Amputation of limbs due to diabetes wounds is a major concern in patients. Other studies interesting on the wound healing efficiency of collagen/alginate scaffolds impregnated with CS- curcumin NPs (196 nm) showed a higher rate of wound healing than the control (sterile gauze) and placebo scaffolds [67]. Further, a synergistic action of curcumin (anti-inflammatory or antioxidant), chitosan (carrier, wound healing activity) and collagen (stimulant for wound healing activity) was persuaded.

The wound healing properties of nanocomposite films was mainly due to their ability to enhance granulation tissue formation, collagen deposition, tissue remodeling and the wound contraction. Zhong et al. [68] reported that chitosan-Ag/ZnO composite dressings enhances the wound healing and promotes re-epithelialization and collagen deposition. Hence, nanocomposite films could be considered as a biodegradable wound dressing, due to their antioxidant and antibacterial properties and wound healing efficiency.

Hydroxyproline Content Determination

Collagen is considered as the most abundant structural protein in the body, contained a high concentration of amino acid hydroxyproline [31]. The hydroxyproline is used historically as a biochemical specific marker for collagen stability and thus for the estimation of rates of collagen synthesis. Data reported in Table 6 revealed an hydroxyproline level of 884.22 mg/g and 742.52 mg/g of tissue for CS-TPP NF4 and CS-TPP NF0 treated groups, respectively, which were significantly ($p < 0.05$) higher than "Cytol basic" (735.16 mg/g of tissue) and control (642.88 mg/g of tissue) groups. Ranjbar and Yousefi [69] reported that hydroxyproline contents increased for the groups treated topically with Aloe vera and dressed with chitosan nanoparticle thin-film membranes (88.54 mg/g) as compared to untreated one (48.77 mg/g). This increase in hydroxyproline content for the treated groups signaled a rise in collagen turnover, which accelerated the wound healing process.

Table 6 Hydroxyproline amounts (mg/g of tissue) in the wound site from the different treated groups

Groups	Hydroxyproline amounts (mg/g of tissue)
Control	642.88 ± 9.78^{a}
Cytol basic	735.16 ± 14.25^{b}
CS-TPP NF0	742.52 ± 18.06^{c}
CS-TPP NF4	884.22 ± 19.81^{d}

Results are expressed as means of three experiments ± SD. Different superscripts (a–d) in the same column indicate significant differences ($p < 0.05$)

Consequently, CS-TPP NF4 implied more collagen deposition and could stimulate the wound healing process by modulating the proliferative and remodeling phases of wound healing. Results strongly support the possibility of using nanocomposite films as dressings for wound care application and especially for the diabetic person due to their biodegradability and non-toxicity.

Histological Study

The histological survey of wound tissues excised from the sacrificed animals was performed at the last day (8th day) of treatment. The microscopic photographs taken for the four groups (Fig. 10) showed the tissue sections of wound areas for treated groups using CS-TPP NF0 and CS-TPP NF4 with a normal histology sections. The layers of skin (epidermis and dermis) were clearly identified. A complete re-epithelialization and well formed granulation tissue of epidermis with remarkable neo-vascularization and fewer inflammatory cells were assessed for the treated groups with nanocomposite films. However, in the histological sections of the wound tissues of untreated and "Cytol basic" groups, a poorly structured of the epidermal layers was observed. In addition, the collagen fibers were not very organized. The dermis displays a massive number of inflammatory cells and a prominent hyperemia of capillary blood vessels. It was also shown a markedly formation of collagen and epithelial layer in the tissues, while, lower mature collagen was observed for the control group tissues with the absence of fibrinoids necroses. Li et al. [70] reported that the chitosan-reinforced implants with collagen and nano-hydroxyapatite provided perfect recovery (in 15 weeks) of wounds with appropriate strength and high mineral density.

The natural origin and biocompatibility of CS promoted its use for wound healing because CS fuels homeostasis and expedites tissue renewal. Furthermore, the hydrophilic character and homogenous structure of CS, relative to glycosaminoglycans, serve as an attractive material for a tissue engineering scaffold [71]. Singh et al. [72] showed that

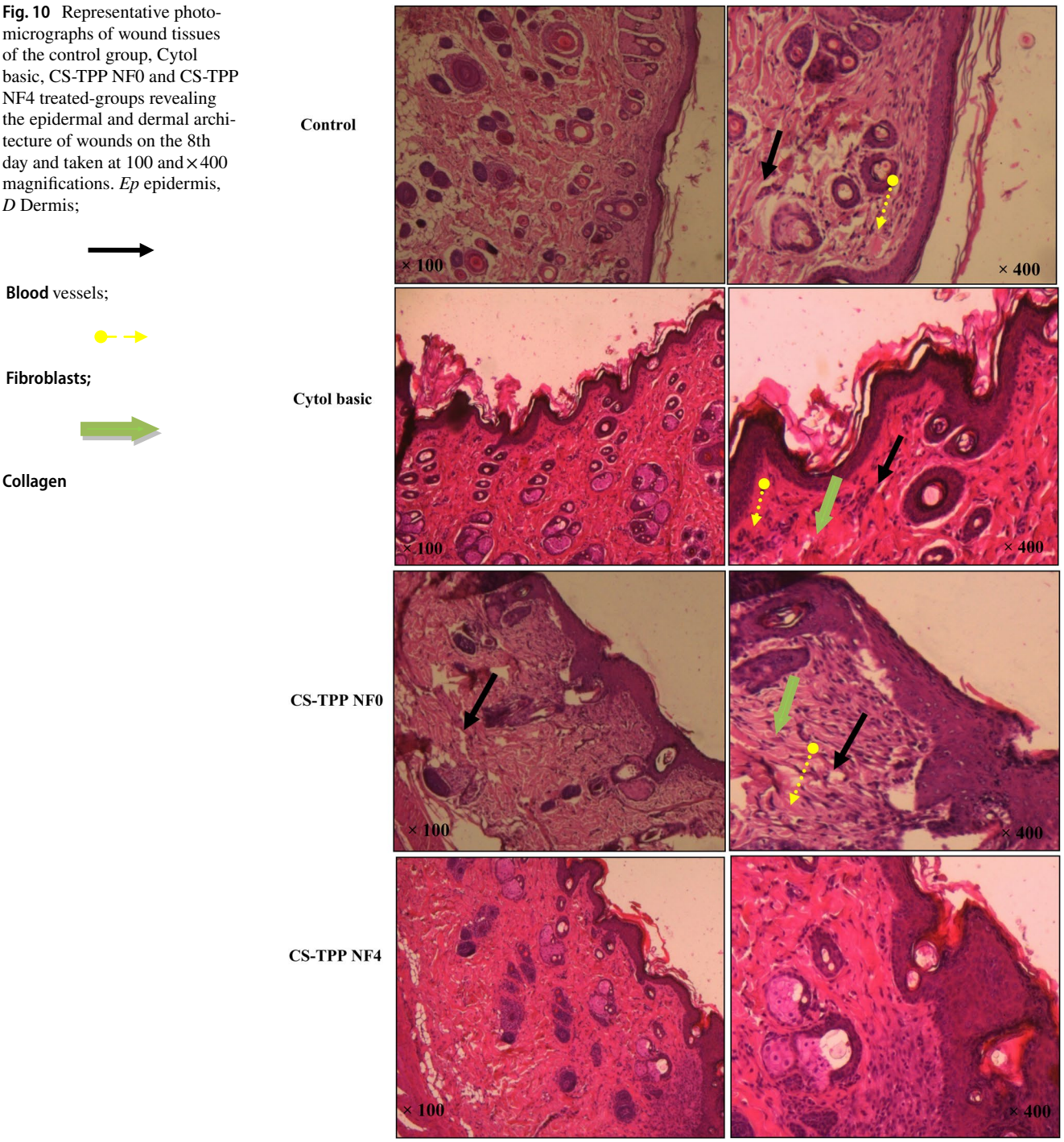

Fig. 10 Representative photomicrographs of wound tissues of the control group, Cytol basic, CS-TPP NF0 and CS-TPP NF4 treated-groups revealing the epidermal and dermal architecture of wounds on the 8th day and taken at 100 and × 400 magnifications. *Ep* epidermis, *D* Dermis;

the CS-NPs with an average diameter of 208 nm and positive zeta potential about 24.2 mV, prepared by ionic gelation method and loaded with calcium alginate hydrogels, exhibited a remarkable antibacterial and pro-inflammatory activity, as indicated by the inhibition of generation of reactive oxygen species. Subsequently, the process promoted vascular endothelial cell invasion, metastasis and neo-vascularization, resulting in a higher rate of wound healing.

In our study, results clearly indicated the potential effects of nanocomposite films in accelerating the wound healing process, as compared to the untreated groups. This process could be due to various effects. Generally, the natural wound healing process was carried out in three phases: the inflammatory phase, the granulation phase (or proliferative stage) and the maturation phase, giving the final appearance of the scar. CS-TPP NFs enhanced the wound healing progression that may be due to the reduction of inflammatory

phase and a rapid transition to the proliferative phase. Csaba et al. [33] showed that CS-TPP nanoparticles were poorly cytotoxic and caused less than 10% cells death and suggest that there are non-toxic. In this context, the tissue scaffolds based on CS-gelatin with the CS-NPs incorporation could be used to protect the injury during the regeneration process and to improve dermal and epidermal tissue regeneration. Membranes were biodegradable, thus their removal was not required at the end of treatment. Therefore, the implantation of biodegradable membranes could be suited for animals, since they completely covered the wound sites, avoiding the bacterial infiltration.

Conclusion

The main purpose of the current study was to incorporate chitosan nanoparticles onto composite films based on chitosan and gelatin used as wound dressings. Control film showed a homogeneous and smooth surface without any roughness, air bubbles and cracks, which indicated interaction between CS and gelatin components. However, with the CS-NPs incorporation, the SEM micrograph showed a heterogeneous surface with small aggregates with a compact and tortuous structure. Indeed, the CS-NPs incorporation improved significantly the water-resistant ability and mechanical properties, as well as the thermal stability of the nanocomposite films. Furthermore, with CS-NPs incorporation, a significant variation in the contact angle and surface free energy of nanocomposite films, dependent on time and film composition, was found. Interestingly, the addition of nanoparticles onto the films matrices improved their antibacterial and antioxidant properties.

Moreover, it was observed that nanocomposite films accelerated the wound healing process as compared to the untreated groups. Further, nanocomposite films exhibited not only the most enhanced effect on wounds healing but also a good healing process quality as well. The developed films enriched with chitosan nanoparticles could facilitate the proliferation of cells and mitigate the bacterial infections. All these properties suggested that the nanocomposite films could be consider as attractive biodegradable wound dressings.

Acknowledgements The present work is supported by the Utique PHC program (Project SeaCoatPack) N°39290YK of Campus France and No 18G0903 of the CMCU funded by the Ministry of Higher Education and Scientific Research of Tunisia and Ministry of Higher Education, Research and Innovation of France and French Embassy in Tunisia. The authors wish to thank the colleagues from the PAM-PAPC Laboratory for the help and precious collaboration, and to thank Engineering School of Materials (ESIREM) of the University of Bourgogne, DIJON for the facilitated access to the equipment and devices. The equipments involved in this work were also co-funded by the Regional Council of Bourgogne–Franche Comté and the "Fonds Européen de Développement Régional (FEDER)".

Declarations

Conflict of interest The authors have no conflict of interest with any company or colleague. The data that support the findings of this study are available from the corresponding author upon request.

References

1. Delavary BM, van der Veer WM, van Egmond M, Niessen FB, Beelen RH (2011) Macrophagesin skin injury and repair. Immunobiology 216:753–762
2. Tsai CY, Woung LC, Yen JC, Tseng PC, Chiou SH, Sung YJ, Liu KT, Cheng YH (2016) Thermosensitive chitosan-based hydrogels for sustained release of ferulic acid on corneal wound healing. Carbohydr Polym 135:308–315
3. Chandika P, Ko SC, Jung WK (2015) Review Marine-derived biological macromolecule-based biomaterials for wound healing and skin tissue regeneration. Int J Biol Macromol 77:24–35
4. Cheng YH, Yang SH, Su WY, Chen YC, Yang KC, Cheng WT, Wu SC, Lin FH (2010) Thermosensitive chitosan–gelatin–glycerol phosphatehydrogels as a cell carrier for nucleus pulposus regeneration: an *in vitro* study. Tissue Eng Part A 16:695–703
5. Mogosanu GD, Grumezescu AM (2014) Natural and synthetic polymers for wounds and burns dressing. Int J Pharm 463:127–136
6. Marei NH, El-Mazny W, El-Shaer A, Zaki KD, Hussein Z, Abd-El-Samie E (2017) Enhanced wound healing activity of desert locust (*Schistocercagregaria*) vs. shrimp (*Penaeus monodon*) chitosan based scaffolds. Int J Biol Macromol 97:23–33
7. Pei Y, Ye D, Zhao Q, Wang X, Zhang C, Huang W, Zhang N, Liu S, Zhang L (2015) Effectively promoting wound healing with cellulose/gelatin sponges constructed directly from a cellulose solution. J Mater Chem. https://doi.org/10.1039/c5tb00477b
8. Jridi M, Sellimi S, Ben Lassoued K, Beltaief S, Souissi N, Mora L, Toldra F, Elfeki A, Nasri M, Nasri R (2016) Wound healing activity of cuttlefish gelatin gels and films enriched by henna (*Lawsonia inermis*) extract. Colloids Surf A. https://doi.org/10.1016/j.colsurfa.2016.10.014
9. Baek S, Park H, Kim M, Lee D (2020) Preparation of PCL/(+)-catechin/gelatin film for wound healing using air-jet spinning. Appl Surf Sci 509:145033
10. Thomas D, Nath MS, Mathew NRR, Philip E, Latha MS (2020) Alginate film modified with aloevera gel and cellulose nanocrystals for wound dressing application: preparation, characterization and in vitro evaluation. J Drug Deliv Sci Technol 59:101894
11. Salari M, Khiabani MS, Mokarram R, Ghanbarzadeh H, Kafil SB (2018) Development and evaluation of chitosan based active nanocomposite films containing bacterial cellulose nanocrystals and silver nanoparticles. Food Hydrocoll 84:414–423
12. Hajji S, Salem R, Hamdi M, Jellouli K, Ayadi W, Nasri M (2017) Nanocomposite films based on chitosan-poly(vinyl alcohol) and silver nanoparticles with high antibacterial and antioxidant activities. Process Saf Environ Prot 111:112–121
13. Islam MM, Zaman A, Islam MS, Khan MA, Rahman MM (2014) Physico-chemical characteristics of gamma-irradiated gelatin. Prog Biomater 3:21
14. Ooi SY, Ahmad I, Amin MCIM (2016) Cellulose nanocrystals extracted from rice husks as a reinforcing material in gelatin hydrogels for use in controlled drug delivery systems. Ind Crop Prod 93:227–234

15. Lu B, Wang T, Li Z, Da F, Li L, Tang F, Yu K, Liu J, Lan G (2016) Healing of skin wounds with a chitosan–gelatin sponge loaded with tannins and platelet-rich plasma. Int J Biol Macromol 82:884–891
16. Patel S, Srivastava S, Singh MR, Singh D (2018) Preparation and optimization of chitosan-gelatin films for sustained delivery of lupeol for wound healing. Int J Biol Macromol 107:1888–1897
17. Levi-Polyachenko N, Jacob R, Day C, Kuthirummal N (2016) Chitosan wound dressing with hexagonal silver nanoparticles for hyperthermia and enhanced delivery of small molecules. Colloid Surf B 142:315–324
18. Bugnicourt L, Alcouffe P, Ladavière C (2014) Elaboration of chitosan nanoparticles: Favorable impact of a mild thermal treatment to obtain finely divided, spherical, and colloidally stable objects. Colloid Surf A 457:476–486
19. Riegger BR, Baurer B, Mirzayeva A, Tovar GEMM (2018) Bach systematic approach for preparation of chitosan nanoparticles via emulsion crosslinking as potential adsorbent in wastewater treatment. Carbohydr Polym 180:46–54
20. Wang Y, Li P, Tran TTD, Zhang J, Kong L (2016) Review manufacturing techniques and surface engineering of polymer based nanoparticles for targeted drug delivery to cancer. Nanomaterial 6:26
21. Suresh L, Brahman PK, Reddy KR, Bondili JS (2018) Development of an electrochemical immune sensor based on gold nanoparticles incorporated chitosan biopolymer nanocomposite film for the detection of prostate cancer using PSA as biomarker. Enzyme Microb Technol 112:43–51
22. Shao J, Wang B, Li J, Jansen JA, Walboomers XF, Yang F (2019) Antibacterial effect and wound healing ability of silver nanoparticles incorporation into chitosan-based nanofibrous membranes. Mater Sci Eng C 98:1053–1063
23. Zhao R, Li X, Sun B, Zhang Y, Zhang D, Tang Z, Chen X, Wang C (2014) Electrospun chitosan/sericin composite nanofibers with antibacterial property as potential wound dressings. Int J Biol Macromol 68:92–97
24. Yousefi I, Pakravan M, Rahimi H, Bahador A, Farshadzadeh Z, Haririan I (2017) An investigation of electrospun Henna leaves extract-loaded chitosan based nanofibrous mats for skin tissue engineering. Mater Sci Eng C 75:433–444
25. Hajji S, Younes I, Ghorbel-Bellaaj O, Hajji R, Rinaudo M, Nasri M, Jellouli K (2014) Structural differences between chitin and chitosan extracted from three different marine sources. Int J Biol Macromol 65:298–306
26. Bkhairia I, Bardaa S, Ktari N, Ben Abdallah Kolsi R, Kallel R, Zghal S, Ben Salah R, Nasri M (2018) Gelatins from *Liza aurata* skin: Structural characterization, *in vitro* and *in vivo* validation of acceleration epithelialization and cyto-protective effect. Polym Test. https://doi.org/10.1016/j.polymertesting.2018.09.012
27. Hafsa J, Smac MA, Ben Khedher MR, Charfeddine B, Limem K, Majdoub H, Rouatbi S (2016) Physical, antioxidant and antimicrobial properties of chitosan films containing *Eucalyptus globulus* essential oil. LWT - Food Sci Technol 68:356–364
28. Hajji S, Hamdi M, Boufi S, Li S, Nasri M (2019) Suitability of chitosan nanoparticles as cryoprotectant on shelf life of restructured fish *surimi* during chilled storage. Cellulose 26:6825–6847
29. Owens DK, Wendt RC (1969) Estimation of the surface free energy of polymers. J Appl Polym Sci 13:1741–1747
30. Karbowiak T, Debeaufort F, Voilley A (2006) Importance of surface tension characterization for food, pharmaceutical and packaging products: a review. Crit Rev Food Sci Nutr 46:391–407
31. Agarwal PK, Singh A, Gaurav K, Goel S, Khanna HD, Goel RK (2009) Evaluation of wound healing activity of extracts of plantain banana (*Musa sapientum var. Paradisiaca*) in rats. Indian J Exp Biol 47:32–40
32. Lee KH, Tong TG (1968) Studies on the mechanism of action of salycylates II. Retardation of wound healing by aspirin. J Pharm Sci 57:1042–1043
33. Csaba N, Koping Hoggard M, Alonso MJ (2009) Ionically cross linked chitosan/tripolyphosphate nanoparticles for oligonucleotide and plasmid DNA delivery. Int J Pharm 382:5–14
34. Cerchiara T, Abruzzo A, Ñahui Palomino RA, Vitali B, De Rose R, Chidichimo G, Ceseracciu L, Athanassiou A, Saladini B, Dalena F, Bigucci F, Luppi B (2016) Spanish Broom (Spartium junceum L) fibers impregnated with vancomycin loaded chitosan nanoparticles as new antibacterial wound dressing: preparation, characterization and antibacterial activity. Eur J Pharm Sci. https://doi.org/10.1016/j.ejps.2016.11.028
35. Li J, Huang Q (2012) Rheological properties of chitosan-tripolyphosphate complexes: from suspensions to microgels. Carbohydr Polym 87:1670–1677
36. Hu B, Pan C, Sun Y, Hou Z, Ye H, Zeng X (2008) Optimization of fabrication parameters to produce chitosan-tripolyphosphate nanoparticles for delivery of tea catechins. J Agric Food Chem 56:7451–7458
37. Servat-Medina L, González-Gómez A, Reyes-Ortega F, Oliveira Sousa IM, Almeida Queiroz NDC, Wiziack Zago PM, Jorge MP, Monteiro KM, de carvalho JE, San Román J, Foglio MA, (2015) Chitosan–tripolyphosphate nanoparticles as Arrabidaea chica standardized extract carrier: synthesis, characterization, biocompatibility, and antiulcerogenic activity. Int J Nanomed 10:3897–3909
38. Zamora-Mora V, Fernández-Gutiérrez M, San Román J, Goya G, Hernández R, Mijangos C (2014) Magnetic core-shell chitosan nanoparticles: rheological characterization and hyperthermia application. Carbohydr Polym 102:691–698
39. Teramoto N, Hayashi A, Yamanaka K, Sakiyama A, Nakano A, Shibata M (2012) Materials 5:2573–2585
40. Huster D, Schiller J, Arnold K (2002) Comparison of collagen dynamics in articular cartilage and isolated fibrils by Solid-State NMR spectroscopy. Magn Reson Med 48:624–632
41. Kanmani P, Dhivya E, Aravind J, Kumaresan K (2014) Extraction and analysis of pectin from citrus peels: augmenting the yield from *Citrus limon* using statistical experimental design. Iran J Energy Environ 5:303–312
42. Hajji S, Chaker A, Jridi M, Maalej H, Jellouli K, Boufi S, Nasri M (2016) Structural analysis, and antioxidant and antibacterial properties of chitosan-poly (vinyl alcohol) biodegradable films. Environ Sci Pollut Res 23:15310–15320
43. Jridi M, Hajji S, Ben Ayed H, Lassoued I, Mbarek A, Kammoun M, Souissi N, Nasri M (2014) Physical, structural, antioxidant and antimicrobial properties of gelatin–chitosan composite edible films. Int J Biol Macromol 67:373–379
44. Muyonga JH, Cole CGB, Duodu KG (2004) Extraction and physicochemical characterization of Nile Perch (*Latesniloticus*) skin and bone gelatin. Food Hydrocoll 18:581–592
45. Le Tien C, Letendre M, Ispas-Szabo P, Mateescu MA, Delmas-Patterson G, Yu LH, Lacroix M (2000) Development of biodegradable films from whey proteins by cross-linking and entrapment in cellulose. J Agric Food Chem 48:5566–5575
46. Jingou J, Shilei H, Weiqi L, Danjun W, Tengfei W, Yi X (2011) Preparation, characterization of hydrophilic and hydrophobic drug in combine loaded chitosan/cyclodextrin nanoparticles and *in vitro* release study. Coll Surf B 83:103–107
47. Ibezim C, Andrade CT, Marcia C, Barretto B, Odimegwu DC, DeLi FF (2011) Malonically cross-linked chitosan/TPP microparticles for the controlled delivery of pyrimethamine. Ibnosina J Med BS 3:77–88
48. Rubentheren V, Ward TA, Chee CY, Tang CK (2015) Processing and analysis of chitosan nanocomposites reinforced with chitin

whiskers and tannic acid as a crosslinker. Carbohydr Polym 115:379–387
49. Taravel MN, Domard A (1995) Collagen and its interaction with chitosan: II. Influence of the physicochemical characteristics of collagen. Biomaterials 16:865–871
50. De Moura MR, Lorevice MV, Mattoso LHC, Zucolotto V (2011) Highly stable, edible cellulose films incorporating chitosan nanoparticles. J Food Sci 76:25–29
51. Yin Y, Li Z, Sun Y, Yao K (2005) A preliminary study on chitosan/gelatin polyelectrolyte complex formation. J Mater Sci 40:4649–4652
52. Chang PR, Jian R, Yu J, Ma X (2010) Fabrication and characterization of chitosan nanoparticles/plasticised-starch composites. Food Chem 120:736–740
53. De Moura MR, Aouada FA, Avena-Bustillos RJ, Mc Hugh TM, Krochta JM, Mattoso LHC (2009) Improved barrier and mechanical properties of novel hydroxypropyl methylcellulose edible films with chitosan/tripolyphosphate nanoparticles. J Food Eng 92:448–4533
54. Martelli MR, Barros TT, de Moura MR, Mattoso LH, Assis O (2013) Effect of chitosan nanoparticles and pectin content on mechanical properties and water vapor permeability of banana puree films. J Food Sci 78:98–104
55. Banach M, Makara A (2011) Thermal decomposition of sodium phosphates. J Chem Eng Data 56:3095–3099
56. Hosseini SF, Rezaei M, Zandi M, Ghavi FF (2013) Preparation and functional properties of fish gelatin-chitosan blend edible films. Food Chem 136:1490–1495
57. Tang CH, Jiang Y (2007) Modulation of mechanical and surface hydrophobic properties of food protein films by transglutaminase treatment. Food Res Int 40:504–509
58. Rehman MAU, Munawar MA, Schubert DW, Boccaccini AR (2019) Electrophoretic deposition of chitosan/gelatin/bioactive glass composite coatings on 316L stainless steel: a design of experiment study. Surf Coat Technol 358:976–986
59. Zhang Z, Cheng X, Yao Y, Luo J, Tang Q, Wu H, Lin S, Han C, Wei Q, Chen L (2016) Electrophoretic deposition of chitosan/gelatin coatings with controlled porous surface topography to enhance initial osteoblast adhesive responses. J Mater Chem B 4:7584–7595
60. Mao JS, Cui YL, Wang XH, Sun Y, Yin YJ, Zhao HM, De Yao KA (2004) preliminary study on chitosan and gelatin polyelectrolyte complex cytocompatibility by cell cycle and apoptosis analysis. Biomaterials 25:3973–3981
61. Karbowiak T, Debeaufort F, Champion D, Voilley A (2006) Wetting properties at the surface of iota-carrageenan based edible films. J Colloid Interface Sci 294:400–410
62. Zhan F, Sheng F, Yan X, Zhu Y, Jin W, Li J, Li B (2017) Enhancement of antioxidant and antibacterial properties for tannin acid/chitosan/tripolyphosphate nanoparticles filled electrospinning films: Surface modification of sliver nanoparticles. Int J Biol Macromol 104:813–820
63. Melo N, MendonçaSoares B, Diniz K, Leal C, Canto D, Flores M, da Costa T-F, Galembeck A, Montenegro T, Montenegro Stamford-Arnaud T, Stamford C (2018) Effects of fungal chitosan nanoparticles as eco-friendly edible coatings on the quality of postharvest table grapes. Postharvest Biol Technol 139:56–66
64. Whitesides GM (2005) Nanoscience, nanotechnology, and chemistry. Small 1:172–179
65. Qi L, Xu Z, Jiang X, Hu C, Zou X (2004) Preparation and antibacterial activity of chitosan nanoparticles. Carbohydr Res 339:2693–2700
66. Wang T, Zheng Y, Shen Y, Shi Y, Li F, Su C, Zhao L (2018) Chitosan nanoparticles loaded hydrogels promote skin wound healing through the modulation of reactive oxygen species. Artif Cells Nanomed Biotechnol 46:138–149
67. Karri VVSR, Kuppusamy G, Talluri SV, Mannemala SS, Kollipara R, Wadhwani AD, Mulukutla S, Raju KRS, Malayandi R (2016) Curcumin loaded chitosan nanoparticles impregnated into collagen-alginate scaffolds for diabetic wound healing. Int J Biol Macromol 93:1519–1529
68. Zhong L, Jingting G, Qingfeng H, Jie W, Donghui L, Hao Y, Rong C (2016) Enhanced antibacterial and wound healing activities of microporous chitosan-Ag/ZnO composite dressing. Carbohydr Polym 156:460–469
69. Ranjbar R, Yousefi AR (2018) Effects of aloe vera and chitosan nanoparticle thin-film membranes on wound healing in full thickness infected wounds with methicillin resistant *Staphylococcus Aureus*. Bull Emerg Trauma 6:8–15
70. Li XM, Feng QL, Liu XH, Dong W, Cui FH (2006) Collagen-based implants reinforced by chitin fibres in a goat shank bone defect model. Biomaterials 27:1917–1923
71. Ahmed S, Ikram S (2016) Chitosan based scaffolds and their applications in wound healing. Achiev Life Sci 10:27–37
72. Singh A, Mittal A, Benjakul S (2021) Chitosan nanoparticles: preparation, food applications and health benefits. Sci Asia 47:1–10